2020-01-01

Density Functional Calculations On Single Molecular (1d) And Van Der Waals Bi -Layered (2d) Magnets.

Md Shamsul Alam
University of Texas at El Paso

DENSITY FUNCTIONAL CALCULATIONS ON SINGLE MOLECULAR (1D) AND VAN DER WAALS BI -LAYERED (2D) MAGNETS.

MD SHAMSUL ALAM

Master's Program in Computational Science

APPROVED:

Rajendra Zope, Ph.D., Chair

Tunna Baruah, Ph.D.

Suman Sirimulla, Ph.D.

Ahmed El-Gendy, Ph.D.

Stephen L. Crites, Jr., Ph.D.
Dean of the Graduate School

Dedication

I dedicate this Thesis to my mother Shahida Akhter and my father Md Alamgir Majumder.

DENSITY FUNCTIONAL CALCULATIONS ON SINGLE MOLECULAR (1D) AND VAN DER WAALS BI-LAYERED (2D) MAGNETS.

by

Md Shamsul Alam

THESIS

Presented to the Faculty of the Graduate School of

The University of Texas at El Paso

in Partial Fulfillment

of the Requirements

for the Degree of

MASTER OF SCIENCE

Computational Science Program

THE UNIVERSITY OF TEXAS AT EL PASO

August 2020

Acknowledgements

I express my heartiest gratitude to the Almighty Allah and heartfelt thanks for the blessing, guidance, protection and help in all aspects of my life. It is my great pleasure to express my utmost gratitude to my teacher, and supervisor of this thesis work Prof Dr. Rajendra Zope, Department of Physics, University of Texas at El Paso. It was an extraordinary experience for me to work under his supervision in such a well-equipped lab. I am truly indebted to him for allowing me to work in this laboratory. His constant guidance, valuable suggestions, encouragement, innovative ideas and new innovative techniques was the driving force behind the success of the research work. I thank him for everything he did and for helping me for completion of this work. I would also like to express my deepest thanks to my venerable teacher and Co-supervisor Prof Dr Tunna Baruah, Dept. of Physics, University of Texas at El Paso, for her guidance, thoughtful suggestions, continuous encouragement and assistance have been a great source of inspiration throughout the progress of my research work. I would like to offer her my utmost gratitude. Special thanks to Dr. Chang Pohao, Dr Luis Basurto, and Dr Yoh Yamamoto for their utmost help, encouragements, critical comment and cordial dealings throughout the research. I am really thankful to my friend and lab mates Prakash Mishra, Selim Romero and Peter for their co-operation and supportive company throughout the research work.

Abstract:

Low-dimensional magnetic materials show novel properties that is not seen in bulk magnets. The weak interactions such as spin-orbit interactions, electron correlation, van der Waals interaction in case magnetic bi-layers, play an important role in determining the properties of the system. Using density functional theory, we computationally investigated two categories of magnetic material- 1: Single Molecular Magnets (SMM) 2: Van der Waals layered Cr-Halide magnets. We used different classes of density functionals to examine the spin ordering and magnetic anisotropy barriers in several single molecule magnets - Mn_{12}, Co_4, Ni_4, V_{15}. We find that the magnetic anisotropy barrier significantly depends on the choice of the functional and also on the structure. On our second part of the project we perform calculations on bi-layered systems $CrBr_3$and CrI_3. To treat the correlated d-orbitals of the Cr^{3+}we perform GGA+U correction in order to capture correct electronic properties of the system. Also, our theoretical calculation suggests that that van-der-Waals (vdW) functionals which is non-local exchange correlation function of vdW-DF represent the vdw interaction between the stack of layers and the generalized gradient approximation (GGA-PBE) are inadequate for the description of vdW interactions. We also report comparative study of the MAE, and magnetic exchange interaction (J) with respect to pressure up to 1GPa.

Table of Contents

List of Tables:

List of Figures:

Chapter 1: Introduction

Scaling from the bulk dimensions to the smaller units, in which isolated molecules and collection of molecules can exhibit magnetic properties, often referred to the term Molecular Magnetism [1]. At this moment there is tremendous interest in the idea that molecules can store singular bits of data and this could be utilized in ultra-high-density data storage or quantum computing. Historically, these systems have operated at very cold temperature and is not useful in a sort of industrial applications. As we gather an ever-increasing number of data that needs to be stored - particularly in the immense banks of Internet search engines - enormous amounts of energy are being used to power the storage facilities and, yet further, to keep them cool. It has been found that Single molecular magnets (SMM) have potential applications in high density digital storage device and an entire arrangement of data stored in sub-atomic bits would assist us with retreating from a potential crisis - however an impediment to this is the intensely low temperature that these molecules need to be kept at: 30-40 kelvin. But at the School of Chemistry at the University of Manchester, the research group, led by Dr. David Mills and Dr. Nicholas Chilton have figured out a way to store such molecules at just 60 kelvin (around the boiling point of liquid nitrogen)[2]. It shows that magnetic hysteresis, a memory effect that is a prerequisite of any data storage, is conceivable in individual molecules at 60 K. This is close to the temperature of liquid nitrogen (77K). The outcome implies that data storage with single molecules could become a reality in the light of fact that the data servers could be cooled using relatively cheap liquid nitrogen at 77K instead of far more expensive liquid helium (4.15 K). This is substantially more reasonable and could signify a leap towards a progressive technology. In this study, we focus on concentrating about SMM which are often called atomic nano magnets.

1.1: A Brief about SMM

Single-molecule magnets (SMM) are compounds consisting of correlated metal ion and organic ligands that exhibit magnetic stability below a certain 'blocking' temperature. In contrast to traditional magnetic materials, SMM are organic or inorganic/organic hybrid materials, comprised of metal containing spin units. This temperature is mainly determined by the energy required to switch between two opposite orientations of the molecule's magnetic moment. A key factor is the metal ion's magnetic anisotropy which is the extent to which the ion's response to a magnetic field depends on the direction of the field. [1]. In 1967 Wickman et al. [3] reported the first molecule-base magnet, [Fe(dtc)2Cl] (monochlorobis(diethyl-dithio-carbamato) iron(III), which has a S=3/2 ground state and the critical temperature is 2.46 K. After that, there is a 10-year span without any further activity. In 1987 Miller, Epstein, and their co-workers [4] synthesized another molecule that ferromagnetically orders at Tc= 4.8 K. After this discovery, some more molecule-based magnets have been reported, including some that order at room temperature [5]. The above molecule-based magnets results from the intermolecular interaction and have large regions, called domains, that have their spins correlated due to intermolecular magnetic exchange interactions.

Single molecule magnets have been extensively studies in recent years because of both scientific and practical reasons [6][1]. For these magnetic species, the size of them becomes such small that each crystallite behaves as a single domain. Recently, the first single molecular magnet is synthesized by Lis et al . It contains 12 manganese atoms; the four-minority spin Mn (IV) atoms form a cube at the center of the molecule and eight majority spin Mn (III) atoms form a crown around the inner cube. And the inner four Mn (IV) ions are ferromagnetically coupled to each other and the eight outer crown Mn (III) ions are also ferromagnetically coupled. But these two types of ions are antiparallel with each other and this leads this molecule possessing total spin S=10 ground state [8×2−4×3/2=10] and magnetic moment of 20 μ B. This molecule has a very low critical temperature below 3 K but has a very high energy barrier around 60∼62K [7]. In spite of this, a lot of experiments suggest that the spin system is somehow able to overcome this barrier at low temperatures [1] . Below 3 K, steps are observed in the hysteresis loop of powder sample [8] and single crystals [9] .From the crystalline field or coordinator theory, the orbital contribution to the magnetic moment is partially quenched by the symmetry and the anisotropy is commonly expressed with an effective spin Hamiltonian:

$$H = DS_z^2 + E(S_z^2 - S_z^2) + g\mu_B S \cdot H$$

The first term is the axial anisotropy corresponding to the energy barrier between states, say, “spin up” and “spin down”, second term is the transverse second-order magnetic anisotropy and the last term is the Zeeman interaction. For a molecule with uniaxial symmetry, E=0. The anisotropy constant D is known to be negative so that the Sz= ±10 levels lie lowest in energy, while the Sz=0 level lies highest. As there is no external field, the microstates with the same absolute value (|Sz|=±10) have the same energy, the pairs with the same energy level can tunnel each other and a short cut of the barrier occurs to accelerate the magnetic relaxation. This quantum tunneling happens when two microstates (spin up and spin down) with different spin number have the same energy. For example, a spin up microstate will directly flip into the spin down state without climbing the anisotropy barrier. This quantum property of superposition of these two states is used in the idea of quantum computing. When external field is applied, the energy coincident between two states will vanish and the quantum tunneling effect is suppressed. But at some field strength, the energy coincident happens again. So, it is very important to investigate the anisotropy energy of the molecules, which comes from the spin-orbital coupling. A stable single molecular magnet must have a high anisotropy energy, which prevent different microstates to flip through thermally activated and it must have a large spin for the ground state. The three necessities for a particle to be a SMM are: (1) a generally large spin S for the ground state; (2) an obvious negative magneto-anisotropy, for example a prevailing zero-field splitting (zfs) term, D^2S_z ($D < 0$), in the spin Hamiltonian; and (3) not very large of value for the tunnel splitting of the ground state. The large spin and negative magneto-anisotropy decide the magnitude of the thermodynamic barrier for classical thermal activation, leading to reversal of the direction of magnetization for a molecule. It is imperative to stress that, regardless of whether an specific complex have a large barrier for magnetization reversal, it may not function as a SMM if the complex has a quick pace of quantum tunneling of the direction of its magnetization. To make future applications more feasible: Raising of the anisotropy energy is an absolute necessity.

1.2: Spin and the idea of making a quantum Bit

Although our study does not focus on implementation of SMM in quantum computing but it is important to computationally search for perfect candidate material suitable in the area of quantum computing and a thorough study of the magnetic properties of those material can certainly enhance the steps towards the future of quantum computing.

To find the prime factors of a 2048-bit number it would take a classical computer millions of years. A quantum computer can do it in minutes and that is because quantum computers is built on qubits, these devices which take advantage of quantum superposition to reduce the number of steps required to complete the computation. But how is a qubit made in practice and how do you read and write information. Researchers of Fundamental Quantum Tech Lab use outermost electron in the phosphorous atom as a qubit. This single P atom is embedded in a single crystal right next to tiny transistor [10]. Now the electron has a magnetic dipole called its spin and it has two dimensions, up or down, which are like the classical one and zero.

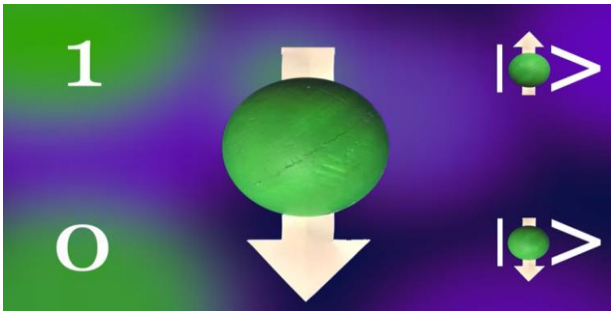

Fig. 1. 1 Up Down spin as classical 1 and 0

To differentiate the energy state when the spin is up and spin down, strong magnetic field needs to be applied. To do that Researchers of Fundamental Quantum Tech Lab used super conducting magnets are used which is a large solenoid- a coil of super conducting wire that sits inside of a water vessel that is full of helium vessel. So now the electrons will line up with its spin pointing down that is its lowest energy state and it would take some energy to put it into the spin up state which is not much energy. But if it were in a room temperature the electron would have so much thermal energy that it would be bouncing around from spin up and spin down. To avoid such activities of spin, the temperature is cooled down to few hundreds of degree above absolute zero

to make sure there is not enough thermal energy in the surroundings to flip it the other way and the spin remains in a single state. So, it is very important to search for molecules which have a high anisotropy barrier. Now if we are to write information onto the qubit we can put the electron into the spin up state by hitting it with a pulse of microwaves which is of very specific frequency and that frequency depends on the magnetic field that the electron is sitting in. Now the electron acts as a radio which can only tune in to one station and when that station is broadcasted the electron gets excited and turns to the spin up state.

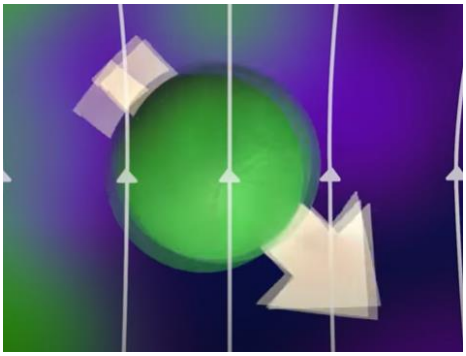

Fig. 1. 2 Excited Spin flipping when magnetic field is applied

1.3: SMM in the areas of Quantum Computing

Energy levels and magnetic quantum states are well defined at the molecular level for molecular magnets. Due to the fact that their basic units contain identical clusters of transition metals, Molecular magnets have actually shown, since the beginning of the 90s, fascinating quantum phenomena, such as the tunnelling of magnetization through an anisotropy barrier and quantum interference (Berry's phase).

It is reported that single spin of SMMS can be treated as a query, so the SMMS which forms a crystal with large spin moments can act as large independent units [6]. Hence several queries can be done within the single crystal. Different ways of Super position of different spin eigen states is necessary. They showed that this query can be implemented in terms of a unitary transformation applied to the single spin of a molecular magnet. Such molecular magnets, forming identical and

largely independent units, are embedded in a single crystal so that the ensemble nature of such a crystal provides a natural amplification of the magnetic moment of a single spin. We can use such spin systems of given *s* to great advantage in building dense and highly efficient memory devices. The well-known Mn_{12} and Fe_8 complexes have a total spin $S = 10$. Below a few kelvin, thermal fluctuations cannot overcome the anisotropy barrier on the scale of hours, and quantum physics sets in. So, the magnetization varies by the transition of discrete energy levels generated from zero field splitting.

1.4: Magnetism and transition metals

As previously discussed, traditional magnetic materials are two- and three-dimensional arrays of inorganic atoms, whose magnetic cores are transition metals, lanthanide metal containing spin units. Most of the transition elements show paramagnetic behavior. The unpaired electrons in (n-1) d orbitals are responsible for the magnetic properties. From Pauli Exclusion Principle we know- Two electron with same energy level must have opposite spins, so their magnetic moments cancel each other. In the case of paired electrons, the electrons in each pair will have opposite spin. The magnetic field created by the electrons of same pair is equal and opposite in nature. Hence the magnetic field which is created by one electron is canceled by the other. So, the net effect of the magnetic moment is zero. Whereas an unpaired electron is regarded as a micro magnet which has a definite magnetic moment. So, some transition elements, lenthanides, and actinides have a net magnetic moment since their energy levels have unpaired electrons.

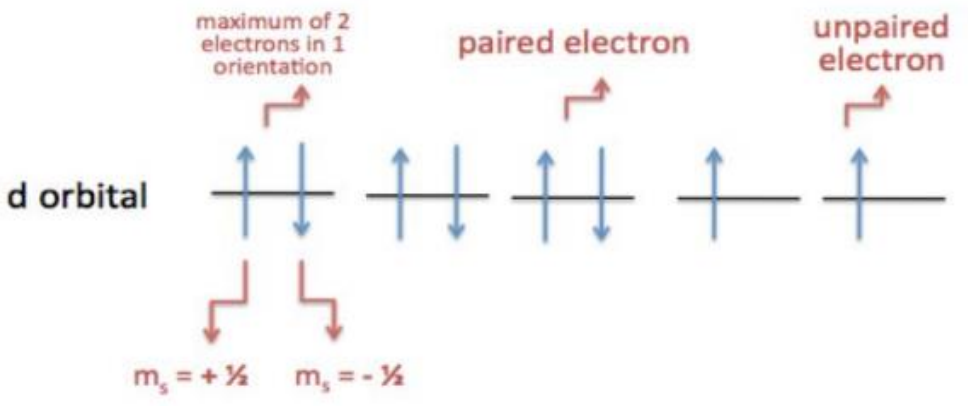

Fig. 1. 3 D orbital energy level following Hund's rule

The reason we focus on transition metal systems with d unpaired electron because P orbitals with unpaired electrons are mostly alkali, which is reactive and those even at their vapor forms are dimers. But liquid oxygen shows paramagnetic behavior because it is attracted by magnetic field and the oxygen has two unpaired electrons. Electrons for their characteristic of revolving around the orbitals and, also spinning in its own axis creates a magnetic field. Unpaired electrons spin with same direction with respect to each other, increases the magnetic field effect.

1.5: Magnetic Anisotropy Energy and Spin Orbit Coupling (SOC)

Magnetic Anisotropy arises from unpaired electrons in a material, molecule or cluster, which are not distributed equivalently in all directions in space. This phenomenon plays a major role in the creation of an energy barrier which separates different microstates with different spin magnetic moment. At a molecular level, there are two sources of magnetic anisotropy: 1) dipolar interactions [11] 2) single-ion anisotropy [12]. Now, we will talk about these two sources independently. Given two electrons in two orbitals with two distinctive energy levels, four ground-state combinations are possible. The combination with both electrons occupation of the lower energy is called singlet state (S=0), and there is only one microstate for S=0 and the other three combination structures a triplet state (S=1, ms=0, ±1). When there is no external field, all three triplet-states are degenerate. Assumed we compress this molecule towards certain direction, for example, z-axis, the electrons experience a more prominent repulsion when they are in XZ (state T_y) and YZ (state Y_x) plane than when they are in XY (state Tz) plane. In this way, the degeneracy of triplet states is lifted. The electrons in plane XY will have a low energy, but state T_y and T_x have the same energy; the splitting energy is given by parameter D and has a unit of energy. Moreover, in the event that we extend this molecule along x-axis,the result is that the degeneracy of T_x and T_y is expelled; the electrons in XZ plane endure less repulsion than in YZ plane. This energy difference between states T_x and T_y is characterized by parameter E. The below Fig.4. shows the energy splitting due to dipolar interaction.[13]

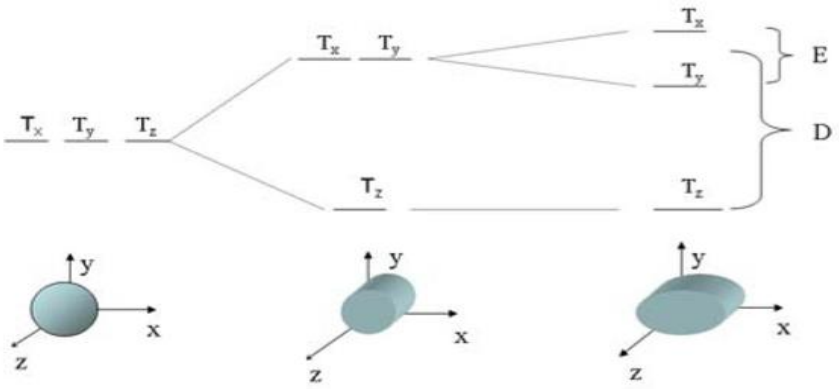

Fig. 1. 4 Schematic picture of energy splitting due to dipolar interaction

Another source of magnetic anisotropy is single-ion anisotropy. In transition metal systems, both dipolar interactions and single-ion anisotropy contribute to the total anisotropy. However, the anisotropy caused by dipolar interactions is quite weak, comparing to single-ion anisotropy. The free ion has an orbital moment if there are unpaired electrons in inner shell for this ion. But this orbital degeneracy can be partially quenched by the crystal field or the ligand field environment. However, there still remains some orbital moment, which comes from the orbital degeneracy. Single-ion anisotropy results mainly from spin-orbital coupling on the ion. The concept of orbital degeneracy is that there are two or more orbitals that can be interconverted by rotation about a suitable axis. For a free transition metal ion, d orbitals form five-fold degeneracy. The d_{xz} and d_{yz} orbitals can be interconverted by rotation 90^o about z-axis, so that if an electron were initially in the d_{xz} orbital it could circulate about the z-axis by jumping between them alternately, which can be easily seen in below fig. 5. This circulation is equivalent to a current flowing and so it produces an orbital moment. Therefore, there would exist an extra spin-orbital coupling term.

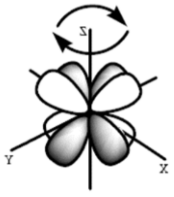

Fig. 1. 5 d_{xz} and d_{yz} orbitals can be interconverted by rotation 90^o about z-axis, as if an electron is hopping between these two orbitals

Chapter 2: Theory

2.1: Density Functional Theory

DFT is one of the most popular and successful quantum mechanical approaches to matter. In its most basic form, it is simply solving Schrödinger's Equation. All information about a given system is contained in the system's wave function, Ψ. The nuclear degrees of freedom (e.g., the crystal lattice in a solid) appear only in the form of a potential v(**r**) acting on the electrons, so that the wave function depends only on the electronic coordinates. This wave function is calculated from Schrödinger's equation, which for a single electron moving in a potential v(**r**) is

$$\left[-\frac{\hbar^2\nabla^2}{2m}+v(\boldsymbol{r})\right]\psi(\boldsymbol{r})=\epsilon*\psi(\boldsymbol{r})$$

If there is more than one electron (i.e., one has a many-body problem) Schrödinger's equation becomes

$$\left[\sum_i^N\left(-\frac{\hbar^2\nabla_i^2}{2m}+v(\boldsymbol{r_i})\right)+\sum_{i<j}U(\boldsymbol{r_i},\boldsymbol{r_j})\right]\psi(\boldsymbol{r_1},\boldsymbol{r_2},\dots,\boldsymbol{r_N})=E\psi(\boldsymbol{r_1},\boldsymbol{r_2}\dots,\boldsymbol{r_N})$$

where N is the number of electrons and $U(\boldsymbol{r_i},\boldsymbol{r_j})$ is the electron-electron interaction.

In a multi-electron system, the number of electrons per unit volume in a given state is the electron density for that state. Its formula in terms of Ψ is

$$\rho(\boldsymbol{r})=N\int|\Psi(\boldsymbol{r}_1,\boldsymbol{r}_2\cdots r_N)^2d\boldsymbol{r}_1\cdots d\boldsymbol{r}_N$$

with a condition

$$\int\rho(\boldsymbol{r})d\boldsymbol{r}=N$$

Hohenberg and Kohn proved that if the ground state is non-degenerate, its total energy could be calculated by the electron density $\rho(\boldsymbol{r})$.

$$E=E[\rho(\boldsymbol{r})]=\int d\boldsymbol{r}\rho(\boldsymbol{r})V_{ext}(\boldsymbol{r})+F[\rho(\boldsymbol{r})]$$

The functional F[ρ(**r**)] consists of three parts:

$$F[\rho(\boldsymbol{r})] = T[\rho(\boldsymbol{r})] + E_H[\rho(\boldsymbol{r})] + E_{xc}[\rho(\boldsymbol{r})]$$
$$[\rho(\boldsymbol{r})] = \frac{1}{2}\int d\boldsymbol{r}\rho(\boldsymbol{r})V_H[\rho(\boldsymbol{r})] = \frac{1}{2}\int d\boldsymbol{r}\rho(\boldsymbol{r})\int d\boldsymbol{r}'\frac{\rho(\boldsymbol{r}')}{|\boldsymbol{r}-\boldsymbol{r}'|}$$

$T[\rho(\boldsymbol{r})]$ is the kinetic energy and E_H is the Hartree energy coming from the electrostatic interaction of the electron. The last term is the exchange correlation energy, which contains all the contributions which is not taken into account by the first two terms, such as spin-orbital coupling. In 1965, Kohn and Sham [P. Hohenberg and W. Kohn. Inhomogeneous Electron Gas. Phys. Rev., 136, B864, 1964] improved it into a practical method by representing the density $\rho(\boldsymbol{r})$ in terms of normalized single-particle orbitals $\varphi_i(\boldsymbol{r})$ with occupation number n_i:

$$\rho(\boldsymbol{r}) = \sum_i^{occ} n_i|\varphi_i(\boldsymbol{r})|^2$$

With condition:

$$\sum_i^{occ} n_i = N$$

So now the total energy in terms of $\varphi_i(\boldsymbol{r})$

$$E = \sum_i^{occ} n_i\int d\boldsymbol{r}\varphi_i^*(\boldsymbol{r})[-\frac{\nabla_i^2}{2} + V_{ext}(\boldsymbol{r}) + \frac{1}{2}V_H[\rho(\boldsymbol{r})]]\varphi_i(\boldsymbol{r}) + E_{xc}[\rho(\boldsymbol{r})]$$

This equation leads to a eigenvalue problem called the Kohn-Sham equation:

$$[-\tfrac{\nabla_i^2}{2} + V_{ext}(\boldsymbol{r}) + V_H[\rho(\boldsymbol{r})] + V_{xc}[\rho(\boldsymbol{r})]]\varphi_i(\boldsymbol{r}) = \varepsilon_i\varphi_i(\boldsymbol{r})$$

$$V_{xc}[\rho(\boldsymbol{r})] = \frac{\delta E_{xc}[\rho(\boldsymbol{r})]}{\delta\rho(\boldsymbol{r})}$$

The operator used in the equation depends on the density $\rho(\boldsymbol{r})$ and thus related to single-electron orbital $\phi_i(\boldsymbol{r})$, which we wish to calculate, so Kohn-Sham equation have to be solved by SCF (Self Consistent Field).

2.2: Exchange Correlation Functional:

The E_{xc} term can be represented as exchange and correlation parts and can be written in terms of the energy per particle, ε_x and ε_c

$$E_{xc}[\rho] = E_x[\rho] + E_c[\rho]$$
$$= \int \rho(\boldsymbol{r})\epsilon_x[\rho(\boldsymbol{r})]dr + \int \rho(\boldsymbol{r})\epsilon_c[\rho(\boldsymbol{r})]d\boldsymbol{r}$$

Assuming that the exchange-correlation energy density at every position in space for the molecule is the same as it would be for the uniform electron gas having the same density as found at that position also known as Local Density Approximation (LDA) functional:

$$E_x^{LDA}[\rho] = C\int \rho^{\frac{4}{3}}(\boldsymbol{r})d\boldsymbol{r}$$

There are several expressions for the correlation energy which have been obtained by fitting to the results of accurate QMC calculations of the uniform electron gas. An improvement in the accuracy provided by the LDA can be obtained by Generalized Gradient Approximation (GGA) functionals. These depend not just on the value of the density at a point (as in the LDA case) but also on its gradient. So we have

$$E_{xc}^{GGA}[\boldsymbol{\rho}] = \int \rho(\boldsymbol{r})\epsilon_{xc}(\rho(\boldsymbol{r}), |\nabla\rho(\boldsymbol{r})|)d\boldsymbol{r}$$

Most GGA (General Gradient Approximation) functionals are constructed in the form of a correction term which is added to the LDA functional

$$\epsilon_{\underset{c}{x}}^{GGA}[\rho] = \epsilon_{\underset{c}{x}}^{LDA}[\rho] + \Delta\epsilon_{\underset{c}{x}}\left[\frac{|\nabla\rho(\boldsymbol{r})|}{\rho^{\frac{4}{3}}(\boldsymbol{r})}\right]$$

The Jacob's Ladder [14] of DFT represented the hierarchy of these approximations with a common expression for the ingredients.

$$E_{xc}[\rho] = \int d^3r\, \rho(\boldsymbol{r})\epsilon_{xc}([\rho], \boldsymbol{r})$$

where $\epsilon_{xc}([\rho], \boldsymbol{r})$ is an energy per electron at point r. The Jacobs ladder of DFT for categorizing the approximations based on the ingredients that the approximations depend on is given below.

Table 1: Functional Taxonomy on the basis of different parameters

DFT E_{xc} Approximations	Ingredients needed for approximation
LSDA	ρ
GGA's	$\rho, \nabla\rho$
Meta-GGA's	$\rho, \nabla\rho, \nabla^2\rho, \tau$
Hybrid Functionals	$\rho, \nabla\rho, \nabla^2\rho, \tau, \psi occ$
RPA	$\rho, \nabla\rho, \nabla^2\rho, \tau, \psi occ, \psi unocc$

The term $\tau = \tau_{\uparrow}+\tau_{\downarrow}$ is the Kohn-Sham kinetic energy density and it is defined as:

$$\tau_\sigma = \frac{1}{2}\sum_{i=1}^{occ} |\nabla\psi_{i\sigma}(\boldsymbol{r})|^2$$

Where, σ is the spin index and the summation i runs over occupied orbitals. The inclusion of τ is for the following reasons. First, it arises naturally in the Taylor expansion of the exact spherically averaged exchange hole near the reference point [15] .Second, the use of τ provides a simple and straightforward way to make a correlation functional exactly one-electron self-interaction free [16]. The inclusion of the kinetic energy density also enables meta-GGAs to have the flexibility to satisfy more exact constraints and thus circumvent the "structure or energy" dilemma experienced by GGAs. The recently developed nonempirical SCAN meta-GGA was constructed to take advantage of the previous discoveries. SCAN is the first meta-GGA that is fully constrained, obeying all 17 known exact constraints that a semilocal functional can. In SCAN, the kinetic energy density τ is used to construct an iso-orbital indicator α which is represented as

$$\alpha = \frac{\tau - \tau^W}{\tau^{unif}} > 0$$

Where, $\tau^W = |\vec{\nabla}\rho|^2/8p$ is the Weizsa¨cker kinetic energy density and the denominator term of the iso-orbital indicator $\tau^{unif} = (3/10)(3\pi^2)^{2/3}\rho^{5/3}$ is the kinetic energy density in the uniform density limit.

Furness and Sun found that in SCAN, the α used with respect to the electron density display divergent behavior at rapidly decreasing electron densities. To make SCAN computationally more stable SCAN functional is modified regularized SCAN (rSCAN) functional has been designed. In the regularization the iso-orbital indicator was modified slightly as

$$\alpha' = \frac{\alpha^3}{\alpha^2 + \alpha_r}$$

Where, $\alpha_r = 1 \times 10^{-3}$, a small constant. The rSCAN functional replaces the problematic region $0 < \alpha < 2.5$ of the switching function f(α) used in

the SCAN functional by a polynomial of degree 7 which removes the oscillatory behavior seen in the exchange correlation potential (V_{xc}) plots.

2.3: Molecular Magnet Mechanisms:

2.3.1: Heisenberg Model:

The Heisenberg model is used to describe the magnetic exchange interaction between the magnetic sites. Considering that only one unpaired electron on each atom contributes the magnetic properties to the system, the Hamiltonian has the following form:

$$\hat{H} = \sum_{i}^{N} \left[-\frac{\nabla_i^2}{2} + V(i)\right] + \sum_{i>j}^{N} \frac{1}{\boldsymbol{r}_{ij}}$$

where, $V(i)$ is the electrostatic potential from the nuclei to this electron. This

Hamiltonian can be decomposed into single-electron Hamiltonian and

electron-electron Hamiltonian:

$$\hat{H}_0 = \sum_{i=1}^{N} \left[-\frac{\nabla_i^2}{2} + V(i)\right] = \sum_{i=1}^{N} \hat{H}_i$$

$$\hat{H}_I = \sum_{i>j}^{N} \frac{1}{\boldsymbol{r}_{ij}}$$

The zero-order approximate wave function can be calculated without the double-electron Hamiltonian:

$$\sum^{N} H_i \Psi = E_0 \Psi$$

The following wave function, product of single-electron wave functions, is one solution satisfying the above equation

$$\Psi_p = \varphi_a(\boldsymbol{r_1}, \sigma_1)\varphi_b(\boldsymbol{r_2}, \sigma_2)|_{\varphi_c}(r_3, \sigma_3) \cdots \varphi_N(\boldsymbol{r_N}, \sigma_N)$$

$\phi_n(r_i, \sigma_i)$ is the single-electron spin orbitals, which can be obtained with single-electron Schrödinger equation:

$$\hat{H}_i \varphi_m(\boldsymbol{r_i}, \sigma_i) = E_m \varphi_m(\boldsymbol{r_i}, \sigma_i)$$

$$\varphi_m(\boldsymbol{r}, \sigma_i) = \mu(\boldsymbol{r_i})\sigma(\sigma = \alpha \text{ or } \beta)$$

For a system with several unpaired electrons, we can construct a wave function with linear combination of several Slater Determinants,

$$\Psi = a_1\Psi_1 + a_2\Psi_2 + \cdots + a_N\Psi$$

Here Ψ_1, Ψ_2, Ψ_3, ⋯, are the slater determinants and a_1, a_2, a_3, ⋯ are the combination coefficients. For a slater determinant, we also can represent with transpositional operator P_v:

$$\Psi_x = \frac{1}{\sqrt{N!}} \sum (-1)^v P_v \Psi_p^X$$

Here, Ψ_X is a slater determinant, and Ψ_p^X is the product of single-electron wave functions. The total energy for a system with wave function as (3.7) will be calculated by:

$$E = \int \Psi^* \hat{H} \Psi d\tau = \sum a_x^* a_y \int \Psi_x^* \hat{H} \Psi_y d\tau$$

Here, X and Y are the indices to the different arrangement single-electron wave functions from a slater determinant. As a result, we get:

$$\int \Psi_X^* \hat{H} \Psi_Y d\tau = \frac{1}{N!} \sum_{v,\omega} \int (-1)^\omega (P_\omega \Psi_p^X)^* \hat{H} \times (-1)^v (P_v \Psi_p^Y) d\tau$$

where ν is the number of exchanging the electrons to get this wave function. The difference between Ψ_p^X and Ψ_p^Y is the spin part of wave function but the spatial part of wave functions is the same. For each Ψ_p^X and Ψ_p^Y, we can separate it into spatial wave function and spin wave function:

$$\Psi_p^X = U_P \chi_p^X \text{ and } \Psi_p^Y = U_p \chi_p^Y$$

So the total energy will have the following form:

$$E = \sum_{X,Y} a_X^* a_Y [E_0 + \sum_{\sigma} \chi_p^{X^*} \hat{H}_{ex} \chi_p^Y]$$

Where,

$$\hat{H}_{ex} = -\frac{1}{2} \sum_{i>j} J_{ij} (I + 4\vec{S}_i \cdot \vec{S}_j)$$

$$J_{ij} = \int \mu_i^*(i) \mu_j^*(j) \frac{1}{r_{ij}} \mu_j(i) \mu_i(j)$$

$$H_{Heisenbergy} = -\sum_{i,j} 2J_{ij} \vec{S}_i \cdot \vec{S}_j$$

Here I is an unit matrix, J_{ij} is called exchange integral and $\mu(i)$ is the space part of single-electron wave function. This is the equivalent Hamiltonian for exchange energy in spin space. [13]

2.3.2: Magnetic Anisotropy

Dr. M. Pederson group in naval research laboratory has developed a simplified but exact method for incorporating spin-orbit coupling into density-functional calculations [17]. The method they introduced is independent of the type of basis set and is applicable to both isolated and periodic systems. Further, there are several computational advantages of this method, i.e. dealing with the standard spin-orbit coupling L·S term without spherical approximation and also, there is no need for the determination of the electric field observed by the moving electrons. The details of this method are presented in the following section.

The classical explanation of spin-orbit coupling is that an electron moving with velocity **v**, in an external electric field E will sense a magnetic field H=**v**×**E**/c. And an electron has spin or intrinsic

magnetic moment, which results in the interaction energy. If we replace external electric field **E** and velocity **v** by the Coulomb potential **Φ(r)** and the momentum operator **P** in order to determine quantum mechanical operator within a Hartree approximation, the Hamiltonian of interaction energy will be as following term:

$$U(\boldsymbol{r},\boldsymbol{P},\boldsymbol{S}) = -\frac{1}{2c^2}\boldsymbol{S}\cdot\boldsymbol{P}\times\boldsymbol{\nabla\Phi}(\boldsymbol{r})$$

Representing the coulomb potential to spherically symmetric term:

$$U(\boldsymbol{r},\boldsymbol{L},\boldsymbol{S}) = \frac{1}{2c^2}\boldsymbol{S}\cdot\boldsymbol{L}\frac{1}{r}\frac{d\Phi(\boldsymbol{r})}{d\boldsymbol{r}}$$

This equation supposes the coulomb potential is spherical and ignores the non-spherical corrections that may be very important for anisotropy energies. The spin-orbit coupling term will be represented as an additional term in Hamiltonian matrix with single-electron wave functions, which are expressed by:

$$\psi_{is}(r) = \sum_{j\sigma} C_{j\sigma}^{is} f_j(\boldsymbol{r})\chi_\sigma$$

Where $f_j(\boldsymbol{r})$ is a spatial basis function, χ_σ is a majority or minority spin spinor and $C_{j\sigma}^{is}$ are determined by diagonalizing the Hamiltonian matrix. In this basis set, the generalized spin-orbit interaction is expressed in term of matrix elements:

$$\begin{aligned} U_{j\sigma,k\sigma'} &= \langle f_j\chi_\sigma|U(\boldsymbol{r},\boldsymbol{P},\boldsymbol{S})|f_k\chi_{\sigma'}\rangle \\ &= \sum_x -\frac{1}{2ic^2}\langle f_j|[\boldsymbol{\nabla}\times\boldsymbol{\nabla\Phi}(\boldsymbol{r})]_x|f_k\rangle\langle\chi_\sigma|S_x|\chi_{\sigma'}\rangle \\ &= \sum_x \frac{1}{i}\langle f_j|V_x|f_k\rangle\langle\chi_\sigma|S_x|\chi_{\sigma'}\rangle \end{aligned}$$

With the operator V_x defined as:

$$\begin{aligned} \langle f_i|V_x|f_j\rangle &= -\frac{1}{2c^2}\left\langle f_i\left|\frac{d}{dy}\frac{d\Phi}{dz}-\frac{d}{dz}\frac{d\Phi}{dy}\right|f_j\right\rangle \\ &= \frac{1}{2c^2}\left(\left\langle\frac{df_i}{dz}|_\Phi\right|\frac{df_j}{dy}\right\rangle-\left\langle\frac{df_i}{dy}|_\Phi\right|\frac{df_j}{dz}\right\rangle\Big) \end{aligned}$$

The matrix elements for V_y and V_z are obtained with the cyclical permutations of the coordinate labels (x→y→z→x). According to the above equation for the spin-orbit coupling matrix. the expression is ideal for basis sets constructed with Gaussian-type functions, Slater functions and plane wave. With the spin-orbit coupling as a perturbation term in Hamiltonian and also consideration of an external magnetic field B, the perturbed wave functions should satisfy:

$$\left[H + \left(\frac{\boldsymbol{V}}{i} + \frac{1}{c}\boldsymbol{B}\right) \cdot \boldsymbol{S}\right] |\psi'_{i\sigma}\rangle = \varepsilon_{i\sigma} |\psi'_{i\sigma}\rangle$$

Here V is the spin-orbital coupling term, *i* is imaginary number. If we denote M=(**V**/*i*+**B**/c), then second order perturbation theory tells us that trace of the Hamiltonian matrix is perturbed by following expression:

$$\Delta = \Delta_1 + \Delta_2$$

$$\Delta_1 = \sum_{x\sigma} S_x^{\sigma\sigma} \sum_{l} \langle \phi_{i\sigma} | M_x | \phi_{i\sigma} \rangle$$

$$\Delta_2 = \sum_{\sigma\sigma'} \sum_{xy} M_{xy}^{\sigma\sigma'} S_x^{\sigma\sigma'} S_y^{\sigma'\sigma}$$

$$M_{xy}^{\sigma\sigma'} = M_{jx}^{\sigma\sigma'^*} = \sum_{ij} \frac{\langle \phi_{i\sigma} | M_x | \phi_{j\sigma'} \rangle \langle \phi_{j\sigma'} | M_y | \phi_{i\sigma} \rangle}{\varepsilon_{i\sigma} - \varepsilon_{j\sigma'}}$$

$$S_x^{\sigma\sigma'} = \langle \chi_\sigma | S_x | \chi_{\sigma'} \rangle$$

here, $\phi_{i\sigma}$ are occupied states and $\phi_{j\sigma}$ are unoccupied states. For uniaxial symmetry the first order energy shift equals to zero, and since the Cartesian off-diagonal M matrices vanish and $M_{xx}^{\sigma\sigma'} = M_{yy}^{\sigma\sigma'}$, the second order contribution to the energy shift becomes:

$$\Delta_2 = \sum_{\sigma\sigma'} \sum_{xy} M_{xx}^{\sigma\sigma'} S_x^{\sigma\sigma'} S_y^{\sigma'\sigma}$$

$$S_x^{\sigma\sigma'} = \langle \chi^\sigma | S_x | \chi^{\sigma'} \rangle$$

If we assume the states (μ1, μ2) = (↑,↓) is parallel to the a specific axis, say, z axis, the most general set of spinors can be expressed by:

$$|\chi_1\rangle = e^{i\gamma}[\cos\frac{\theta}{2}|\uparrow\rangle + e^{i\beta}\sin\frac{\theta}{2}|\downarrow\rangle]$$
$$|\chi_2\rangle = e^{-i\gamma}[-e^{-i\beta}\sin\frac{\theta}{2}|\uparrow\rangle + \cos\frac{\theta}{2}|\downarrow\rangle$$

where θ and β are variational parameters. After performing a bit of algebra, the total energy shift has the following form:

$$\Delta = A + \frac{B}{c}\langle S_z\rangle + \frac{\gamma}{2}\langle S_z\rangle^2$$
$$A = (M_{xx}^{11} + M_{xx}^{22} + M_{zz}^{12} + M_{zz}^{21} + M_{xx}^{12} + M_{xx}^{21})/4$$

$$\gamma = (2/\Delta N^2)(M_{zz}^{11} + M_{zz}^{22} + M_{xx}^{12} + M_{xx}^{21} - M_{xx}^{11} - M_{xx}^{22} - M_{zz}^{12} - M_{zz}^{21})$$

γ is the anisotropy tensor. Once the anisotropy tensor has been diagonalized, the total energy shift can be rewritten as:

$$\Delta = \frac{1}{3}(\gamma_{xx} + \gamma_{xy} + \gamma_{xz})S(S+1)$$
$$+\frac{1}{3}[\gamma_{xz} - \frac{1}{2}(\gamma_{xx} + \gamma_{xy})][3S_z^2 - S(S+1)] + \frac{1}{2}(\gamma_{xx} - \gamma_{xy})(S_x^2 - S_y^2)$$

The anisotropy Hamiltonian splits the (2S+1) spin states and further ignoring the isotropic term S(S+1) and the constant term A it can be expressed as:

$$H = DS_z^2 + E\left(S_x^2 - S_y^2\right)$$

Here, the D and E, which are the anisotropic parameters, can be obtained from the diagonalized γ tensor.

$$D = \gamma_{zz} - \frac{1}{2}\left(\gamma_{xx} + \gamma_{yy}\right) \text{ and } E = \frac{1}{2}\left(\gamma_{xx} - \gamma_{yy}\right)$$

For cubic symmetry D=E=0; For axial symmetry $\gamma_{xx}=\gamma_{yy}$ and E=0 and if D>0 the anisotropy is of the easy-plane type but if D<0 it is of the easy-axis type.

Chapter 3: Results and Computational details

3.1: Computational Details for MAE calculation

In our calculation Naval Research Laboratory Molecular Orbital Library (NRLMOL) code [18] has been utilized in calculations on molecular magnets. Linear combination of molecular orbitals method with a basis of Gaussian-type orbitals is implemented in the code. This methodology is "full-potential" and no muffin-tin or atomic spheres geometry is imposed. It has been applied effectively to compute the electronic and magnetic properties of several molecular nanomagnets[19] [20]. The MAE can be calculated by incorporating the spin-orbit coupling. In many cases the agreement between experiment and the result from the first principles calculation are in well consistent. Thereafter, it is fair by all accounts to provide few details on this specific implementation.

The molecular orbitals were expressed as linear combinations of Gaussian functions centered at the atomic sites. The multicenter integrals are numerically evaluated on a precisely generated variational integration mesh [21]. An effective parallelization makes all-electron calculations possible in an affordable period with more than hundred atoms, which is an essential for useful applications in the area of SMM. The issue of basis optimization in all methods employing localized and fixed basis functions, is solved in NRLMOL by tuning to the arrangements of self-consistent isolated atoms [22]. The numerically computed Self-consistent potentials are least-square fitted to the sum of bare spherical Gaussians or Gaussian-screened 1/r potentials, in order to simplify multicenter integrations. This information of the basis sets and the gaussian representation of the atomic potential is used to generate a numerical variational integration mesh that allows to precisely determine integrals required for calculation of secular matrices, total energies and derivatives according to: $I = \int d\boldsymbol{r} Q(\boldsymbol{r}) = \sum_i \ Q(\boldsymbol{r}_i)\Omega$

where Ωi is the volume associated with point $\boldsymbol{r}_i$. $Q(\boldsymbol{r}_i)$ is often the product of two basis functions with a potential. Errors resulting from numerical integration can easily be checked and controlled by adjusting a few parameters which control the mesh construction. It ought to be underlined that the Gaussian-screened potential are just used to advance the numerical quadrature schemes used for mesh generation. The forces acting on each atom are determined from the Hellmann-Feynman-

Pulay theorem [23][24]. Once the self-consistency is achieved, conjugate-gradient method, or LBFGS method, is used to conduct geometry relaxations after obtaining all the forces acting on each atom. Once the geometry with equilibrium forces are achieved and the Kohn Sham wavefunction [25] is obtained, the magnetic anisotropy energies and other properties (polarizabilities, vibrational frequencies) of the system are computed.

3.1.1: Results for SMM

The simplest form of the anisotropy equation can be represented as axial and transverse anisotropy with their corresponding parameters D and E.

$$H = DS_z^2 + E(S_x^2 - S_y^2)$$

Table 2: Axial anisotropy, Spin (S) for different SMM at different functionals and comparison with the experimental values.

System	S	S^{exp}	D (K)					D^{exp}
			PBE	SCAN	RSCAN	CAP	PKZB	
$Mn_{12}O_{12}(O_2CH)_{16}(H_2O)_4$	10	10	-0.56	-0.40	-0.41	-0.58	-0.50	-0.56
$Fe_4(OCH_2)_2(C_4H_9ON)_6$	5	5	-0.56	-0.27	-0.28	-0.68	-0.48	-0.57
$Co_4(CH_2C_5H_4N)_4(CH_3OH)_4Cl_4$	6	6	-0.79	-1.41	-1.40	-0.92	-0.70	-0.7 - -0.9
$K_6[V_{15}As_6O_{42}(H_2O)]$	0.5	0.5	-0.007	-0.0004	—	-0.007	-0.009	Small
$Cr[N(Si(CH_3)_3)_2]$	1.5	1.5	-2.49	—	—	—	—	-2.66
$Ni_4(CH_2C_5H_4N)_4(CH_3OH)_4Cl_4$	4	4	-0.29	-0.11	-0.12	—	—	-0.6 – 0.8

We present a few case studies of MAE at various functionals. As the SMMs are chosen based on high spin ground state, it is imperative to find the correct spin-ordering of the SMMs from the electronic structure calculations. All our listings suggest correct net spin state as of experimental esteems. For Mn_{12}, Fe_4, Co_4, Ni_4, due to their large anisotropy barriers these systems retain their moment orientation at reasonably high temperatures. The values of the SMM's are negative which denotes the fact that large values of magnetization are favored, and we can speak of an "easy axis". The z-component of the magnetic moment is dominant for all the SMMs recorded in the table. The calculated D-value with PBE functional of Mn_{12}, Fe_4, Co_4, Cr-amide are in excellent agreement with the experimental ones. The only discrepancy is found in the system Ni_4 where the D-value is almost half of the experimental value.

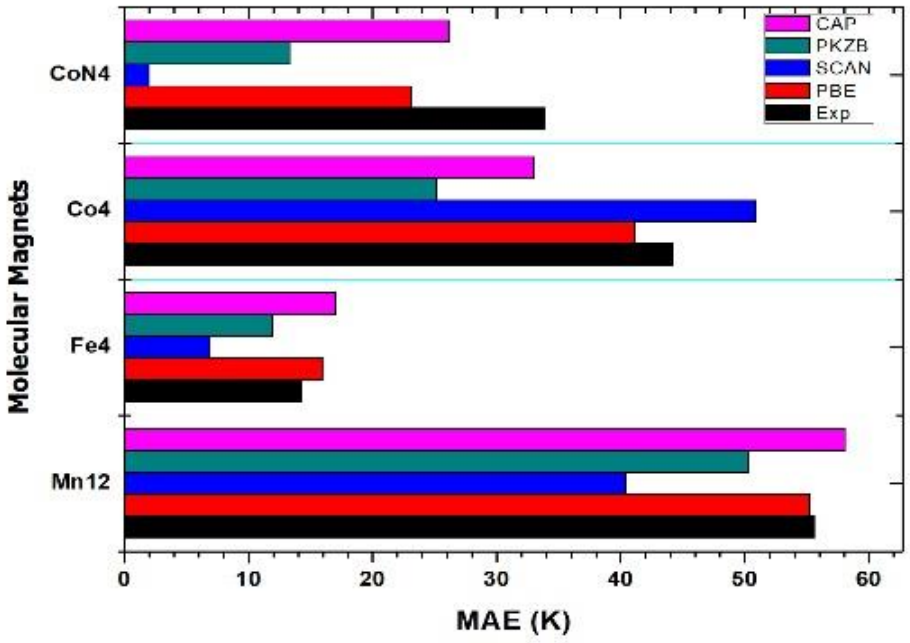

Fig. 1. 6 MAE comparison of SMMs for different functionals denoting PBE to be the best functional in calculating MAE

It is reported that the meta-GGAs attempt to improve upon the LDAs and GGAs by introducing dependence on the kinetic energy density,

$$E_{xc}^{MGGA}[n] = \int dr \epsilon_{xc}(n(r), \nabla n(r), \tau(r))$$

However, to see the performance of the meta-GGA on account of computing MAE we plot the outcomes for the corresponding functionals. Results show that the PBE functionals provides the best depiction of MAE. The SCAN functionals, which is implemented in generalized Kohn-Sham scheme, does not perform well in predicting MAE. From the plots the approximations of MAE aside from the PBE, show dispersed assessments from the experimental values and the deviance of the other functionals from the PBE functional is inconsistent. Though SCAN functional predicts structural and electronic structure accurately, it fails to determine accurate MAE of the SMMs. Also, to ease severe numerical instabilities in generating the pseudopotentials in case for SCAN, rSCAN [26] functional was introduced as a slight modification that replaces the unstable function in SCAN with a numerically stable polynomial function. This modification does not impact any noticeable changes in the MAE. As the adjustment does not affect the HOMO-LUMO gap of a specific system, hence the MAE of SCAN and rSCAN barely shows any significant change. One of the pertinent points for the aberration of the D values for SCAN functionals from the PBE is the HOMO-LUMO (H-L) gap of the system. Considering the system Mn_{12} the H-L gap for PBE is about 0.46 eV and for SCAN the gap is about 0.90 eV which is double the gap of PBE. This discrepancy in the gap is the reason for such deviated estimate of MAE. Although, it appears that a large spin and a small gap will help in enhancing the barrier of the system, we find that it is a subtle transaction between a few different impacts that determines the barrier. For all SMMs we studied here, all the mentioned functionals found the correct spin for all the systems, in agreement with experimentally reported results.

The systems we reported are generally characterized by a high spin ground-state. However, a high spin state does not necessarily correlate with a high anisotropy barrier. The pre-factor D is also very important. In order to increase the barrier one has to understand and control D. The MAE is very sensitive to the geometry changes of the system. Hence, changing the geometry and also maintaining the structural stability for increasing D could be an option.

3.1.2: Brand new molecular design that can endow SMMs larger magnetic anisotropy

The quest for single-molecule magnets (SMMs) with better performance encourages new molecular design that can endow SMMs larger magnetic anisotropy. Two coordinate Co(II) Imido

complexes are outstanding SMM as reported by Yao [27]. Two coordinate Co(II) Imido complexes have highly covalent Co=N cores.

Table 3**: Co(II) Imido complexes and the Magnetic anisotropy parameters**

System	Spin (S)	S_{exp}	Bond length (Co-N)	D (K)
$Co(1)N_3$	1.5	1.5	1.691	-4.82
$Co(2a)N_3$			1.675	-5.06
$Co(2b)N_3$			1.677	-5.55
$Co(3)N_3$			1.682	-6.28

Complex 1 has a near linear C(arene)−N(imido)−Co−C(carbene) alignment and a short Co−N(imido bond (1.691(6) Å).

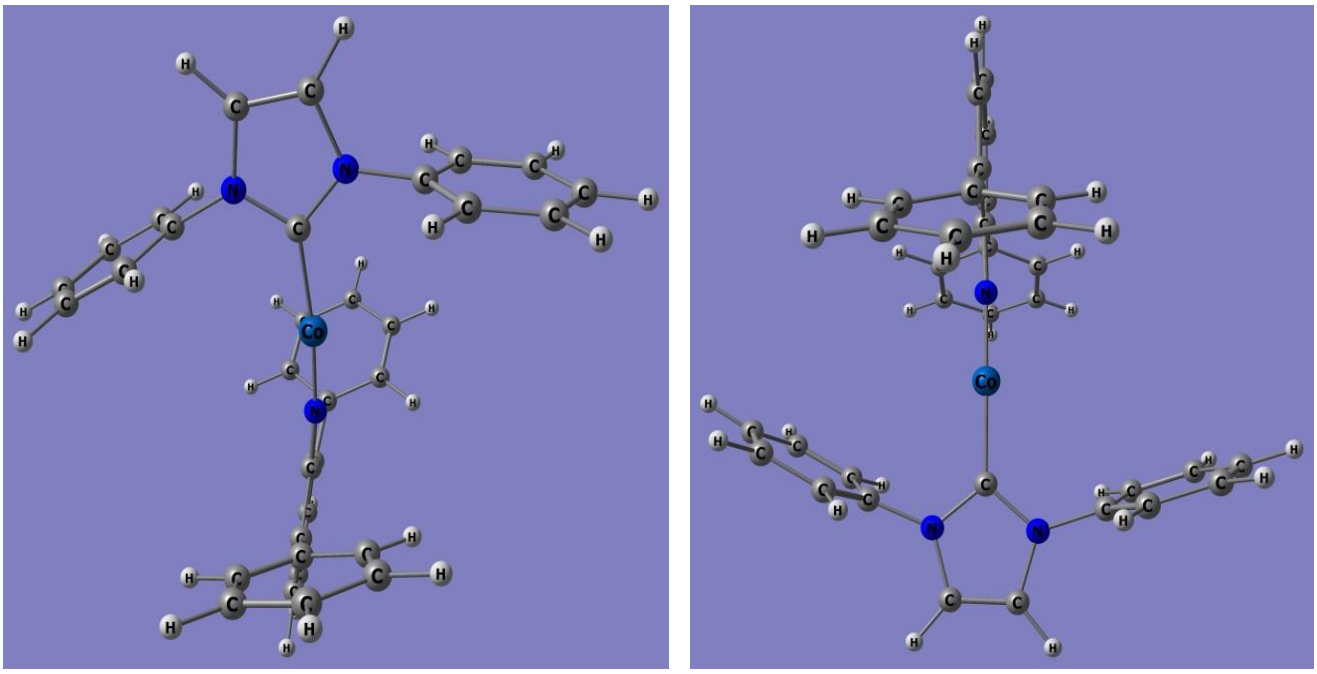

Fig. 1. 7 (a) 3-D visualization of Co(1)N3 complex (b) Co(2a) complex

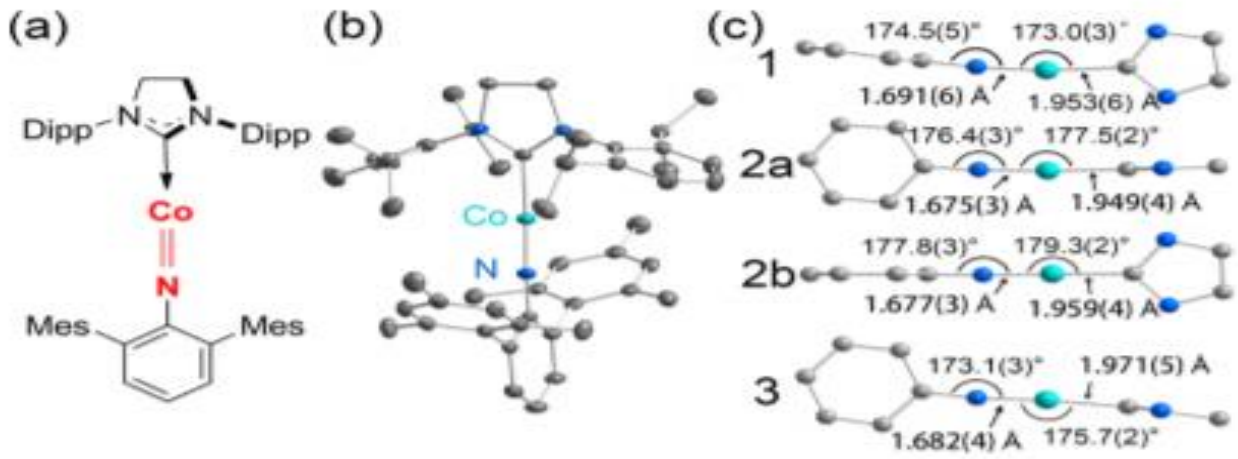

Fig. 1. 8 (a) Schematic structure of [(NHC)CoNDmp] (3 as an example). (b) Molecular structure of 3 CoN (c) Structures of the two-coordinate cores in 1, 2a, 2b, and 3 with key interatomic distances and angles.

The four CoN complexes (1, 2a, 2b, and 3) share the common structural features. The short Co−N(imido) distance is 1.691, 1.675, 1.677, and 1.682 Å for 1, 2a, 2b, and 3, respectively. From the table we can see that upon changing the bond length the MAE can be increased from 10.63 K to 13.24 K. Experimentally anisotropy parameters couldn't be computed correctly, but theoretically computed MAE for Co(II) imidos suggests that these complexes exhibit excellent SMM property and a slight change in the bond length can be used to raise the anisotropy.

In the next part we will study about the single molecular magnet Ni_4 which is not so well studied SMM.

3.1.3: SMM Ni_4

Single Magnetic Molecule $[Ni_4(hmp)_4(CH_3OH)_4Cl_4]$ [28] where hmp is the anion of 2-hydroxymethylpyridine, has similar structure as the SMM Co_4 however Co atoms are replaced by atoms of Ni atoms. In the inner cubic core shown in in fig. 9(b). each Ni_4 molecule comprises four Ni^{2+} (Si = 1) ions coupled through oxygen anions. The net ground state spin is 4 (S= 4×1 alternately occupying the eight corners with S4 symmetry. In this complex there is a $[Ni_4(O\text{-}hmp)_4]^{4+}$ cubane, and each Ni^{II} ion is six coordinate, being bound to three oxygen atoms of the hmp^- ligand, the nitrogen atom of hmp-, one Cl^-, and one CH_3OH atom. The structure has H_2O solvate molecule.

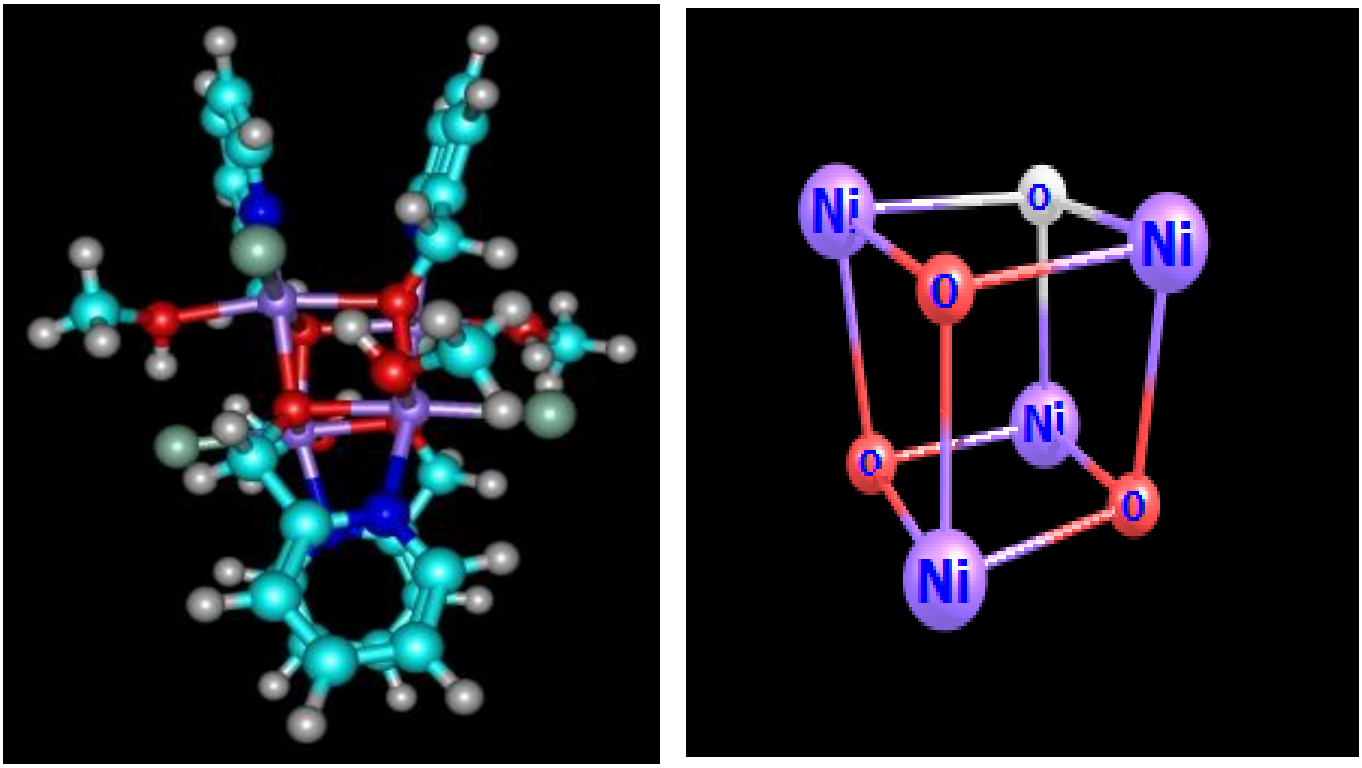

Fig. 1. 9 (a) Geometry of Ni_4 SMM (b) Inner cubic core of 4 Ni^{2+} atoms

The bond separation for Ni_4 are Ni(1)-Ni(2) = 3.161Å, Ni(1)-Ni(3) = 3.23Å, Ni(1)-O(1) = 2.14Å, Ni(2)-O(2)= 2.07 Å and Ni(1)-O(1)-Ni(2) = 98.34°. Experimentally [29] distances for the two different Ni4 molecules in complex 1 are reported 3.026(6) and 3.043(5) Å and Ni(1)-O(1)-Ni(2)= 98.43°. From our calculation the energies of the minority spin LUMO and minority spin HOMO levels are found to be −2.90 and −4.55 eV, while the majority spin LUMO and majority spin HOMO levels are −2.36 and −4.41 eV, respectively. The Fermi energy is −3.66 eV. Our calculation suggests that M_s=4 setup has the lowest energy for this system which is consistent with the experimental result. Hai ping [30] revealed that S=0 ends up being the ground state, trailed by S=2 and S=4. Park [31] reported that total spin of the lowest-energy state to be S = 0, which also does not concur with experiment. Our results with no further approximations incorporated to the DFT calculation resulted in S = 4 as the minimum energy state. The experimental HFEPR data also confirm that Ni_4 complexes have a S=4 ground state and that the axial zero-field splitting parameter D is negative which is exact as our theoretical estimations. Hai-Ping used plane wave basis sets

for the calculation. The plane wave basis sets are delocalized because they are a periodic. Hence, the use of Hubbard U comes into play. A gaussian basis set on the other hand is localized. For the calculation of isolated molecules gaussian basis sets provide better accuracy. The D parameter reported by the theoretical paper of Hai ping and Park is similar to our D parameter which equals to -0.29 K. The negative D denotes that when the temperature of the crystal is decreased, the transitions at the lowest field become the most intense. As we mentioned before in the Ni_4 complexes there are H_2O solvate molecules. Depending on how these H_2O solvate molecules are arranged about Ni_4 molecules and whether some of these H_2O molecules are absent, can result to discrepancies in the local magnetic moments and the MAE. Also, the hmp^- ligand is very sensitive to the temperature that freeze out at the low temperatures in the crystal and its conformations may lead to different Ni_4 molecular environments and play a role in the estimation of MAE.

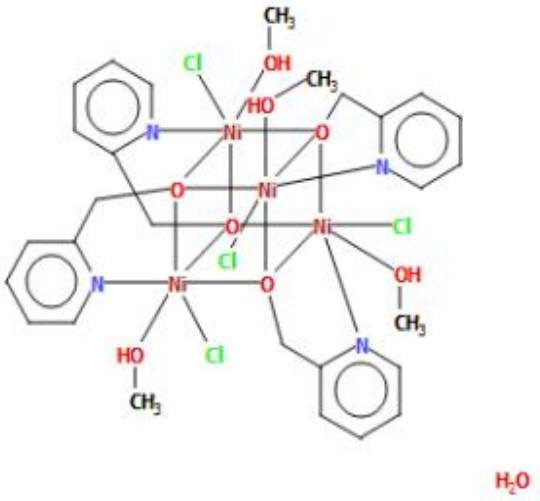

Fig. 1. 10 Missing any Hydrogen combination changes the oxidation state of O in Ch_3OH ligand

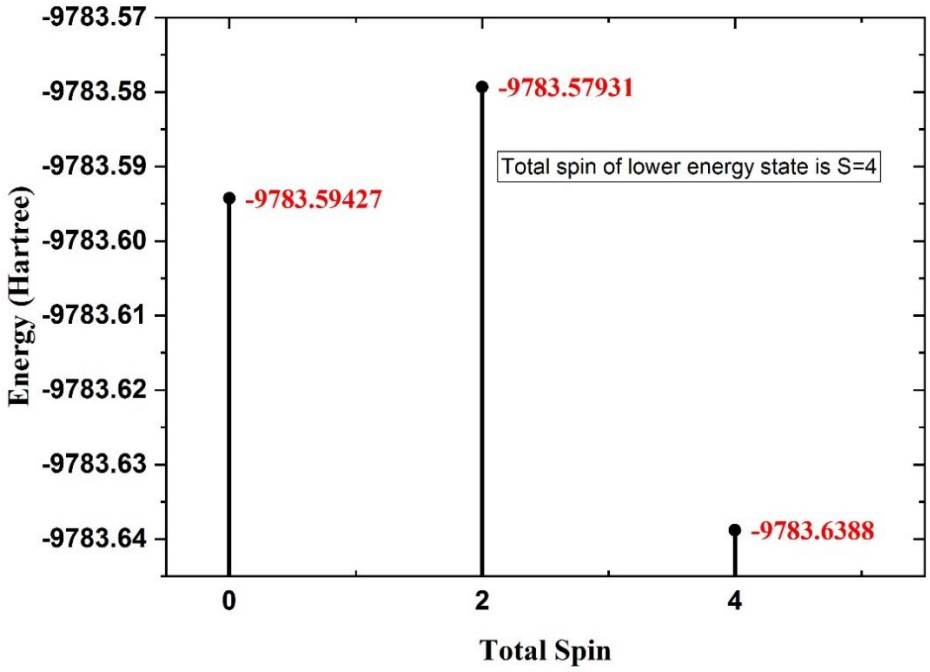

Fig. 1. 11 Energy at different Net spin for Ni_4 SMM showing Net spin of 4 have the lowest energy

Ni_4 molecular magnets are not well separated from each other so that there are four interacting nearest neighboring molecules. To calculate the energies corresponding to different spin configuration, we use the following isotropic Heisenberg exchange Hamiltonian

$$H = -2\sum_{i<j} J_{ij} S_i \cdot S_j$$

which contains the sum over all pairs connected by the different exchange interactions. There are two different types of exchange integral; one has a place with the upper and base faces, say, between Ni(1)-Ni(2) and Ni(3)-Ni(4) and another belongs to the four side faces between Ni(1)-Ni(3), Ni(1)-Ni(4), Ni(2)-Ni(3) and Ni(2)-Ni(4). Then the Heisenberg exchange Hamiltonian changes to

$$H = -2J_1(S_1S_2 + S_3S_4) - 2J_2(S_1S_3 + S_1S_4 + S_2S_3 + S_2S_4)$$

Further, we optimized this 88-atoms molecule with ferromagnetic spin arrangement (S= 4). After that, we changed the spin orientation on Ni and acquired the three energies corresponding to different spin orderings.

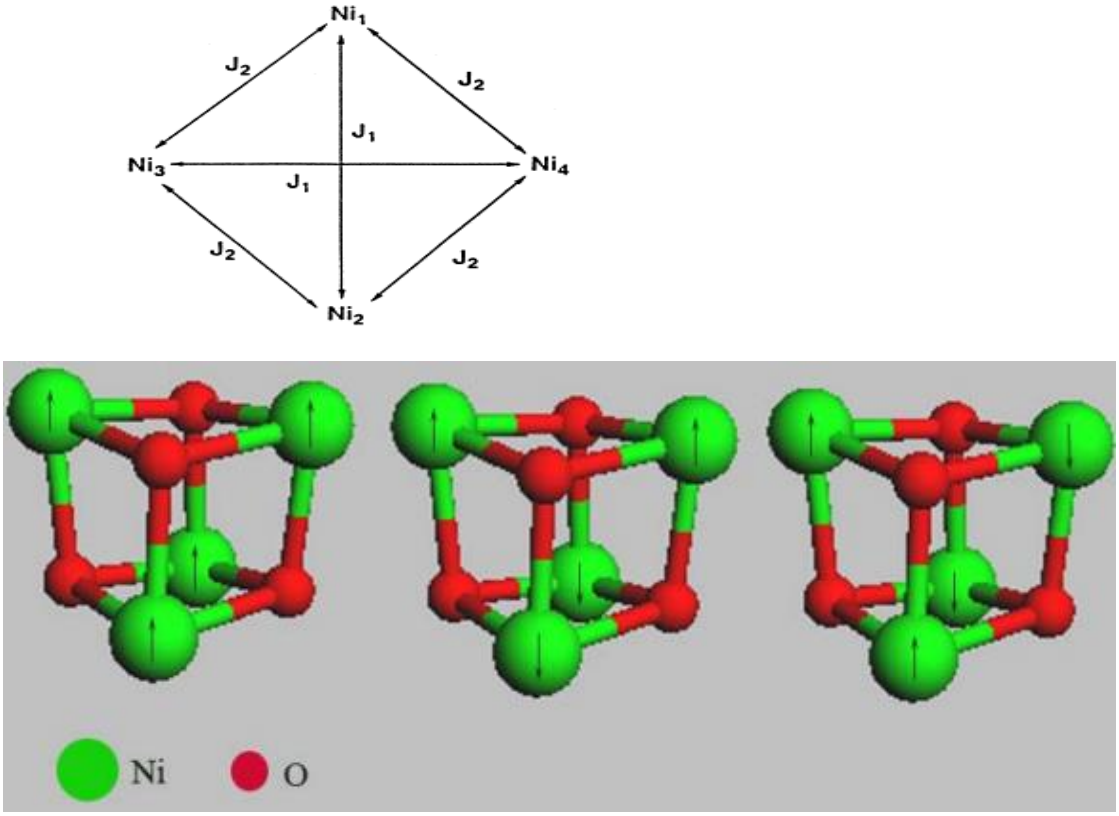

Fig. 1. 12 SMM Ni4 core structure with different spin configurations to calculate exchange coupling

Then the Heisenberg Hamiltonian takes the following form:

Ferromagnet (S_1=S_2=S_3=S_4=1):

$$H_F = -2J_1(2 \times 1 \times 1) - 2J_2(4 \times 1 \times 1) = -4J_1 - 8J_2$$

Antiferromagnet-1 (S_1=S_2=1 and S_3=S_4= -1)

$$H_{AF1} = -2J_1(2 \times 1 \times 1) - 2J_2(-1 - 1 - 1 - 1) = -4J_1 + 8J_2$$

Antiferromagnet-2 (S1=S4=1 and S2=S3=-1)

$$H_{AF2} = -2J_1(-1 \times 2) - 2J_2(-1 + 1 + 1 - 1) = 4J_1$$

With above energy equations, we can get the energy difference:

$$\Delta_1 = (H_F - H_{AF1}) = -16J_2$$
$$\Delta_2 = (H_F - H_{AF2}) = -8J_1 + 8J_2$$

So, the exchange integrals J1 and J2 have the forms as:

$$J_2 = -\frac{1}{16}\Delta_1$$
$$J_1 = -\frac{1}{16}\Delta_1 - \frac{1}{8}\Delta_2$$

We found that the calculated exchange integrals J_1= 4.40 meV and J_2= 0.38 meV which compares well with the experimental results (J_1= 1.14 meV and J_2= 0.34 meV) [29]. The discrepancy between the calculated exchange integrals and experimental results mainly comes from the energies of different spin configurations.

The calculated the anisotropy energy parameters: D = −0.29 and the corresponding experimental results is D= −0.67. The energy barrier between microstate Sz = 4 and Sz = −4 is calculated by E = $|DS_z^2|$= 4.64 K. This means below temperature 4.64 K, the magnetic moments will be frozen.

3.2: Pressure-Induced Vander Waals (vdW) layered Cr Halides

3.2.1: Computational Details

The electronic structure calculations of Van der Waals (vdW) layered system $CrBr_3$ and CrI_3 were carried out with Vienna ab initio (VASP) code [32] within projector augmented-wave (PAW) [33] method. General gradient approximation (GGA) in the Perdew-Burke-Enzerhof (PBE) [34] is used for the exchange correlation functional. The interlayer vdW force is taken into account by including the vdW functional in form of optB88-vdW [35] during the relaxation. A plane wave basis set with cut off 500 eV and for Brillouin zone integration a mesh of 8×8×8 k-points generated by the scheme of Monkhorst-Pack [36] are used. All the lattice constants and ionic coordinates were relaxed until the maximum force on all ions is less than 5×10^{-3} eV/Å. The hydrostatic pressure effect was included by adding the PSTRESS [37] tag adopting the vdW.

3.2.2: Onsite Coulomb Interaction GGA+U

It is known that both LDA and GGA functions tend to over-delocalize d and f states. Such as in Mott insulator where the on-site Coulomb interactions are particularly strong for localized *d* and *f* electrons. The common remedy approach to this shortcoming in these correlated systems is the Hubbard-U method. The Hubbard-U method pioneered by Anisimov et al. [38] introduced an orbital-dependent term known as on-site Coulomb repulsion energy U into the exchange correlation (XC) term of LDA and GGA. They are referred to as LDA + U or GGA + U and expressed as follows

$$E_{GGA+U/LDA+U}[\rho(\boldsymbol{r})] = E_{GGA/LDA}[\rho(\boldsymbol{r})] + E_U[\rho(\boldsymbol{r})] - E_{dc}$$

Here, $\rho(\boldsymbol{r})$ is the electron density, $E_{GGA/LDA}$ is the energy from conventional GGA/LDA functional, E_U is the Hubbard type energy, and E_{dc} is the double-counting correction energy. In this method, the Coulomb energy U and the exchange energy J are combined into a single parameter U-J. GGA + U potentially improves the insufficient description of strongly localized electrons, such as those in Cr-*3d* state, which is previously not correctly described in LDA and GGA.

3.2.3: Results

In chromium trihalides, Cr^{3+} ions are arranged in a honeycomb network in edge-sharing octahedral coordination by six X^- ions, which are each bonded to Cr ions. The layers of composition of CrX_3 are stacked with vdW gaps separating them. To improve the description of 3d states in Cr atoms, the DFT embedded with Hubbard U parameter is used to treat the onsite coulomb interaction on the correlated system.

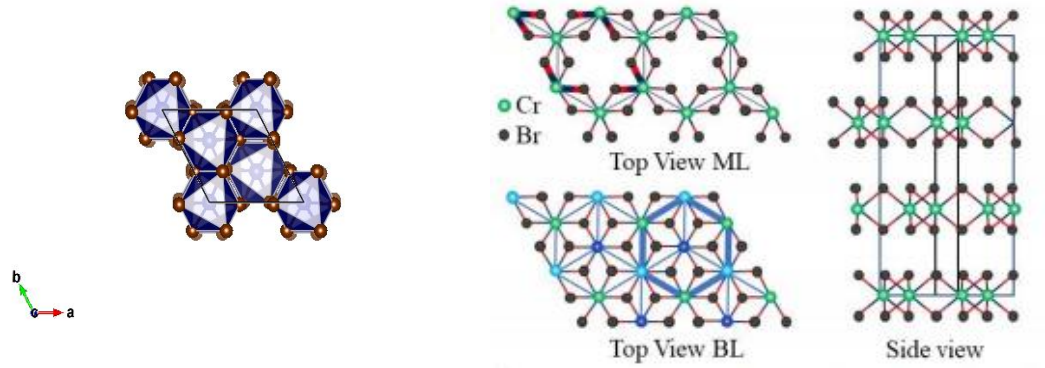

Fig. 1. 13 Crystal Structure of $CrBr_3$

Table 4**: Comparison of Calculated Band gap (BG) with the experimental data for different U values.**

System	U,V (eV)	BG (eV)	Exp BG(eV)
$CrBr_3$	0.0, 0.0	1.35	2.1
	2.7, 0.7	1.80	
CrI_3	0.0, 0.0	0.95	1.1
	2.7, 0.7	1.03	

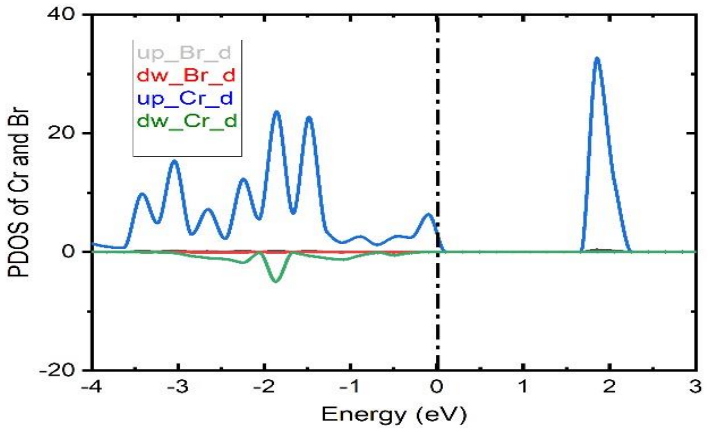

Fig. 1. 14 Partial Density of States (PDOS) for $CrBr_3$ calculated using GGA+U

To investigate the electronic structure for $CrBr_3$. The partial density of states (PDOS) is shown in Fig. 13. The Fermi energy is set to zero where energy region near the Fermi level is mainly composed of the 3d states of Cr^{3+}. From the PDOS of $CrBr_3$ the band gap is about 1.8 eV. The occupied and unoccupied states around the Fermi level are fully spin polarized. The occupied Cr-3d orbitals are only found in the spin-up direction. From Table 5, we can see that +U functional increases the band gap of the system and at U= 2.7 eV J=0.7 eV, the band gap is approximately consistent with the experimental bandgap while it is largely underestimated by the GGA functional. Bulk $CrBr_3$ has a saturated magnetization of ~3μB per Cr^{3+} ion. The magnetic ground state for $CrBr_3$ and CrI_3 are determined by comparing the total energy of different magnetic orderings. Our results suggest that both systems favor FM ordering which are consistent with previous experimental works.

Table 5**: The calculated lattice parameter of $CrBr_3$ and CrI_3 using PBE and optB88-vdW functionals**

System	Lattice Constant (Å)	PBE	optB88-vdW	Experiment[39][40]
$CrBr_3$	a	6.44	6.34	6.26
	c	21.00	18.23	18.2
CrI_3	a	7.00	6.90	6.87
	c	22.40	19.95	19.81

It can be seen from table 5 that both lattice parameters increase from Br to higher element number I. Wei-Bing Zhang [41] reports that the increasing atomic radius of Br/I, change of bond lenths and the weakening reactivity between the Cr and Br/I atoms is the reason for such behavior. Theoretical structural parameters using vdW functional are in good agreement with experimental reports but the PBE overestimated the interlayer distance c by approximately 15%. This exhibits that van der Waals plays a significant role in interlayer binding and optB88-vdW functional computes consistent results.

3.2.4: Hydrostatic Pressure effect

- We have investigated the magnetic properties of layered ferromagnetic $CrBr_3$ and CrI_3 under hydrostatic pressure. Fig. 14a and b displays the pressure dependence of the c/a ratio and volume change. In our computation, both volume and c/a ratio decrease with pressure. It is not surprising that the reduction of c is more significant due to weak interlayer coupling. Similar trend is also observed in several other vdW layered system such as $Cr_2Si_2Te_6$ [42].

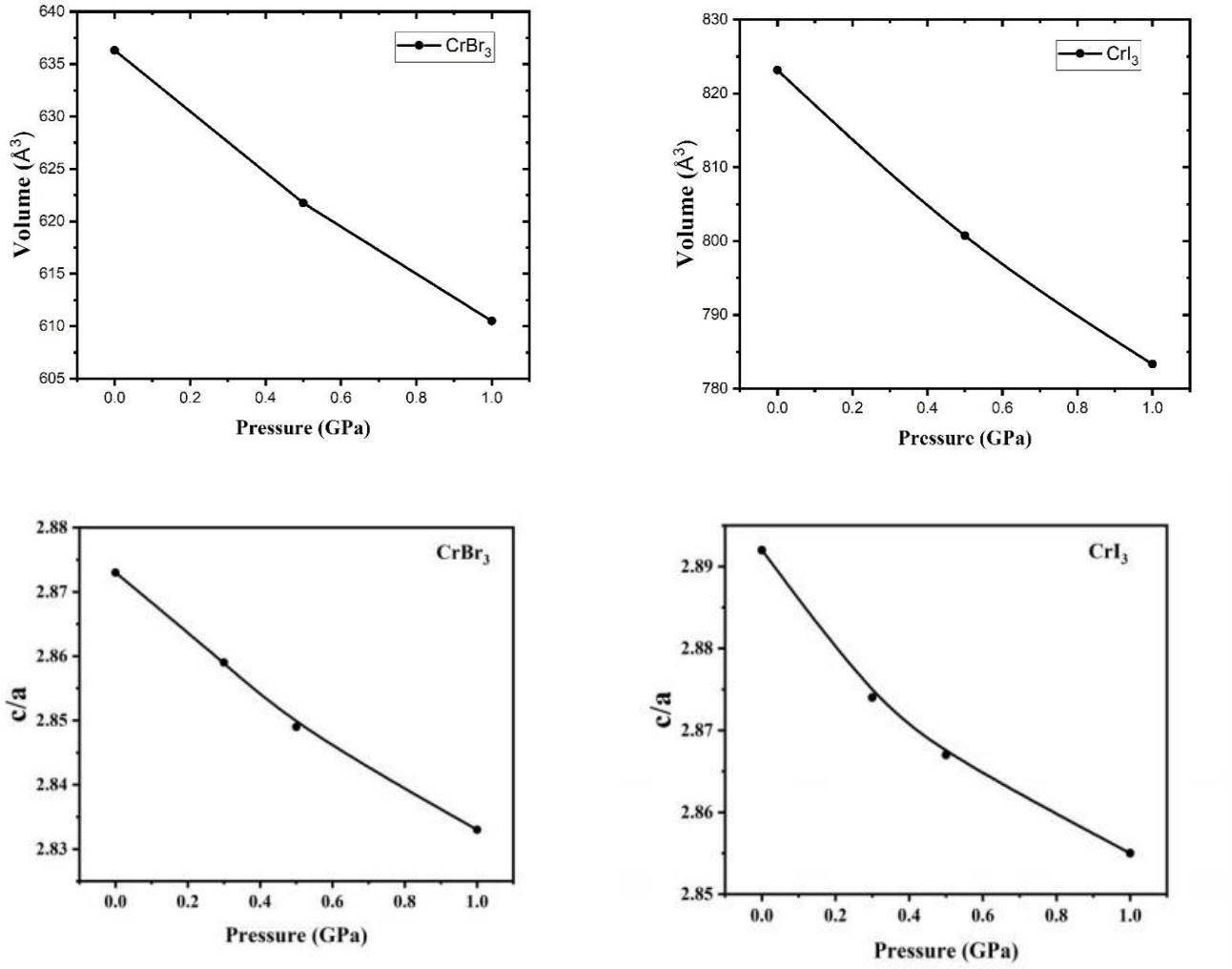

Fig. 1. 15 (a) c/a vs Pressure of $CrBr_3$ and CrI_3 (b) Volume vs Pressure of $CrBr_3$ and CrI_3

To understand how the magnetic properties may vary with applied pressure, two key parameters, exchange coupling J and MAE are considered. As discussed in the previous section, the external pressure changes the lattice constants which influence the inter-site electron hopping process. Two of the common main mechanisms that contribute to the exchange coupling between the localized moments are direct and super-exchange [43]. It is often the result of the competition between the two that dictate the response of the applied pressure. In our model, we consider only the nearest neighbor exchange interaction J_1. The super-exchange interaction which is due to the presence of non-magnetic Br/I in between the Cr ions, increases with the applied pressure and subsequently,

J_1 increases with the isothermal compressibility [44]. Fig. 15 (a) and (b) shows the change of J_1 with pressure.

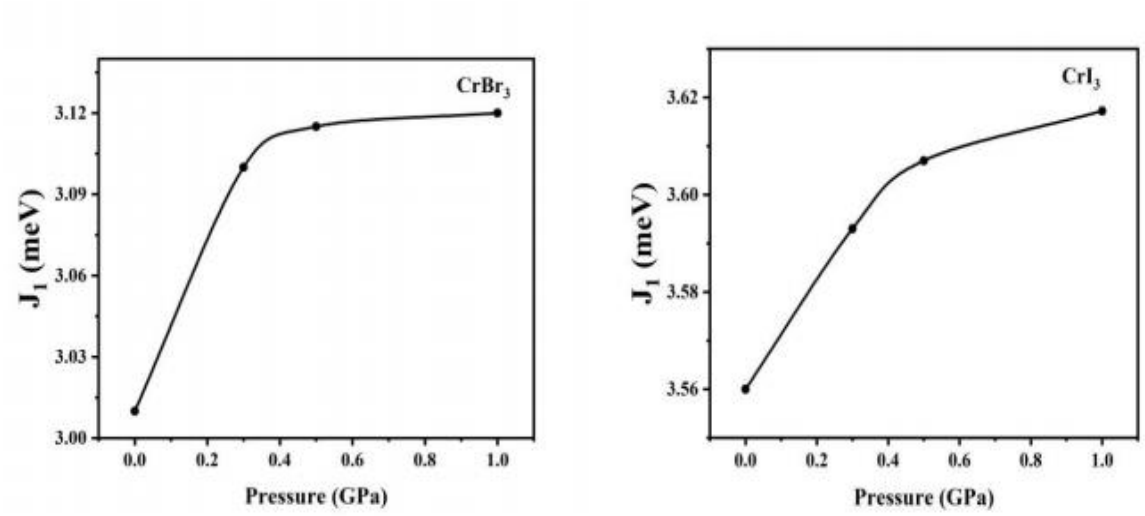

Fig. 1. 16 First nearest neighbor exchange coupling constant J_1 as a function of pressure of (a) $CrBr_3$ and (b) CrI_3 with Hubbard parameter U=2.7eV, J=0.7 eV

This interaction originates due to the virtual hopping of electrons between the two nearest neighbor Cr-ions via I/Br ion. In fig. 15(a) and (b), the plot shows a small but noticeable change due to the applied pressure. It is seen that J_1 increases linearly for P<0.5 GPa while increments are very minimal for $0.5 < P < 1.0$ for both $CrBr_3$ and CrI_3.

Experimentally [45] it is reported for $CrBr_3$ that the Curie temperature (T_C) decreases with pressure and the change of T_C with respect to pressure is about $(dT_C/dP) \sim -0.2$ which implies the negative dependence of J_1 on pressure. From the plot in fig.15(a), we can see an increase of J_1 with respect to pressure depicting an opposite behavior from the experiment. From the theoretical perspective, the FM in-plane super-exchange interaction between the Cr^{3+} in $CrBr_3$ bulk appears to be more dominant than the direct exchange (AFM) interaction which leads to the increase of J_1 value with pressure in the calculation. In the experiment, H. Yoshida claims that the exchange interaction becomes stronger with decreasing atomic distance as there are stronger orbital overlaps [45]. Br certainly have a smaller atomic radius (114 pm) than that of I (133 pm), which might play a role in this dominant Cr-Cr direct exchange interaction. According to the Goodenough-Kanamori-Anderson rule [46], the strength of the delocalization and correlation between the cation-anion-

cation orbitals has a significant impact the exchange interaction behavior. It is probable that $CrBr_3$ have a different correlation effect then that of CrI_3. In order to capture this delocalized behavior in $CrBr_3$ we performed calculation using U=0 eV similar to the calculation done by Adolfo O. Fumega [47].

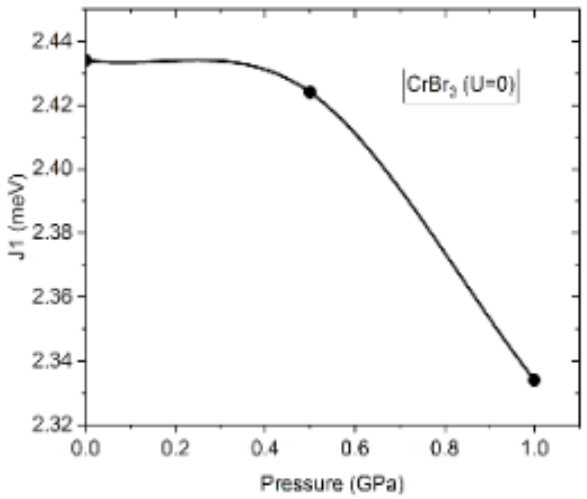

Fig. 1. 17 J_1 vs Pressure without treating the d orbitals of Cr^{3+} in the $CrBr_3$ system

Fig. 16 shows that J_1 decreases with the application of pressure which follows the same pattern as detailed by the experiments. As the pressure increases, the out of plane super exchange between the inter-layers tends to increase resulting in decrease in in-plane super-exchange. This reduction in the in-plane super exchange behavior reduces J_1 as we can see the curve is steeper at J>0.5 GPa. This shows that the Hubbard-U have an influence in the calculations.

The application of pressure affects the bond angle of the Cr-Br-Cr which in turn have effects on the magnetic exchange coupling behaviors. Fig. 17 shows the pressure dependence of the cation-anion-cation angle. The bond angle between Cr-Br-Cr is approximately 90° and decreases with pressure which is in agreement with the recent calculation done by Fumega [43]. The deviation of the bond angle from 90° with pressure also plays major role in the exchange interactions between the magnetic ions. Combining all these effects, the competition between the direct exchange and the indirect super-exchange interaction determine the nature of the J_1 dependence with pressure for $CrBr_3$. The competition between direct exchange through Cr–Cr bonding, which leads to AFM

ordering, and super-exchange through Cr–X–Cr bonding, which leads to FM ordering determine the nature of the J_1 dependence with pressure for $CrBr_3$.

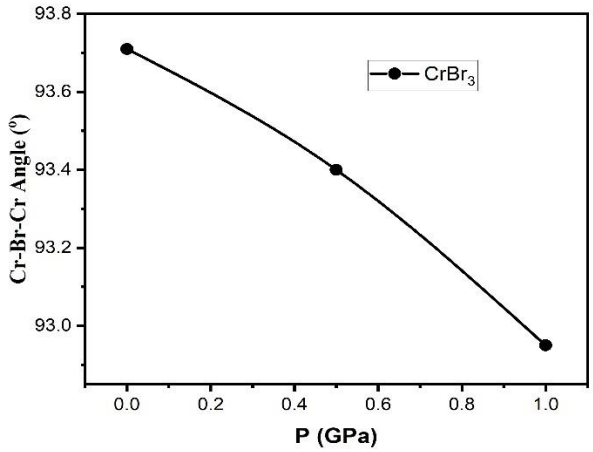

Fig. 1. 18 Reduction of Cr-Br-Cr angle as a function of pressure

In the case of CrI_3 our calculation shows similar behavior with that of $CrBr_3$ with $dJ_1/dP \sim 0.1$ at $0<P<0.5$. Our calculation shows that the reduction of c is relatively more significant than that of a due to the weak interlayer interaction. As the interlayer coupling in CrI_3 is much weaker as compared to other system, the effect of pressure in increasing the coupling between two adjacent layers is much more significant. In bulk CrI_3, the interlayer coupling (J) is FM in nature. Thus, one expects that T_C will increase with the increase in pressure due to the enhancement of interlayer FM coupling. Theoretical calculation done on single layered CrI_3 by Zhang [41] reports that upon applied strain on monolayered $CrBr_3$ and CrI_3, the T_C and interlayer distance increases. While our calculation refers to applying hydrostatic pressure on bulk, its needed to be kept in mind that, applied strain on a monolayer stretches the volume while the pressure on a bulk reduces the system's volume. Our applied pressure on the bulk results in decreasing interplanar distances following the similar trend. Smaller vdW gap, larger in-plane nearest neighbor Cr-Cr distance can enhance T_c, while smaller bond length of Cr-Cr, the increase in interlaying coupling reduces T_c. The role of pressure on J values is very complicated and open question considering the fact that, there are a very few pressure- induced calculations performed especially on the bulk systems.

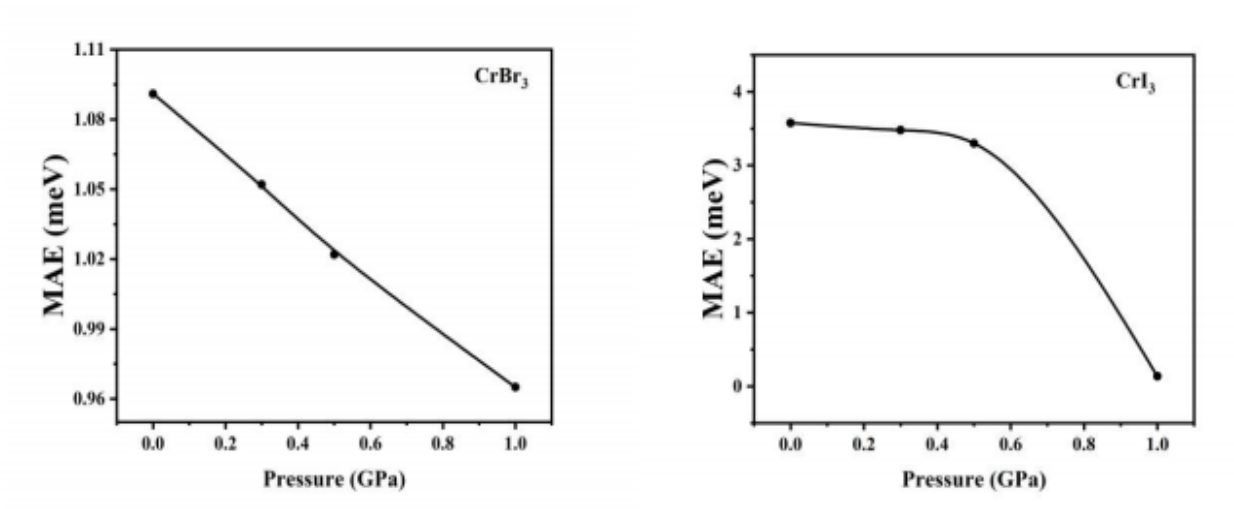

Fig. 1. 19 The magnetic anisotropy vs Pressure of (a) $CrBr_3$ showing no significant changes (b) CrI_3 showing strong suppression of MAE.

As shown in fig 18. MAE is calculated for both bulk $CrBr_3$ and CrI_3 at different pressure which includes the spin orbit coupling (SOC). The easy axis is along the c-direction. Fig. 18 shows bulk CrI_3 have the strongest magnetic anisotropy but CrI_3 undergoes strong suppression of magnetic anisotropy energy with pressure. This behavior agrees with the recent calculation done by Rehab on monolayer $CrBr_3$ and CrI_3 [48]. For $CrBr_3$ as seen from fig. 18(a) there is no significant changes in MAE with respect to pressure. From $CrBr_3$ to CrI_3, the Cr-Cr separation increases with expanding halogen size from Br to I, as a result the direct exchange (overlap between neighboring Cr orbitals) weakens which successively, enhances the covalent nature of Cr-X bond [49]. Therefore, the super exchange interaction and the spin orbit coupling strengthens more for CrI_3 then $CrBr_3$ [48]. Though decrease in MAE results in the decrease of Tc, the change in bond angle and the increase in interlayer coupling could give rise to Tc and hence the MAE and Tc relationship might not be consistent with the general trend observed.

Chapter 4: Summary and discussion:

To summarize, in the initial segment of our thesis, MAE for several molecular magnets at different functionals are calculated. Comparing the MAEs, Mn_{12} have the highest energy barrier and PBE approximation is the best functional to compute consistent MAE. The results suggest that the higher-order contributions to the anisotropy barrier are either due to electronic relaxations that are dependent on spin-orientation, higher-order couplings between scalar relativistic and spin–orbit operators or possibly couplings between electronic and nuclear spins. For Ni_4, we found that the calculated lowest energy state has a total spin of S=4, which is in agreement with the experiment where other theoretical investigation on this specific system failed to determine the correct state. The exchange coupling constant J_1=4.40 meV, J_2=0.38 meV, compared to the experimental value J_1= 1.14 meV and J_2= 0.34 meV. The uniaxial anisotropy parameters are D= −0.29 K. The energy barrier between microstate Sz = 4 and Sz = −4 is calculated by $E = |DS_z^2|$= 4.64 K. Co_4 and Ni_4 have the same structure and Co ions and Ni ions are in the same environment, but Co-based molecule have a high anisotropy energy. To progress towards periodic systems from SMM, we have also studied the magnetic properties of vdW layered $CrBr_3$ / CrI_3 under hydrostatic pressure. For both $CrBr_3$ and $CrBr_3$, J_1 is found to decrease and increase monotonically respectively as pressure increases from 0 to 1.0 GPa. The MAE for both the systems decreases with the application of pressure. The increase of J_1 and the decrease of MAE is more dominant for CrI_3 then $CrBr_3$. The close competition between this super exchange and the direct exchange determines the nature of pressure dependence of T_C in different magnetic systems.

References:

[1] R. Sessoli, "Materials science: Magnetic molecules back in the race," *Nature*, vol. 548, no. 7668, pp. 400–401, 2017, doi: 10.1038/548400a.

[2] C. A. P. Goodwin, F. Ortu, D. Reta, N. F. Chilton, and D. P. Mills, "Molecular magnetic hysteresis at 60 kelvin in dysprosocenium," *Nature*, vol. 548, no. 7668, pp. 439–442, 2017, doi: 10.1038/nature23447.

[3] H. H. Wickman, A. M. Trozzolo, H. J. Williams, G. W. Hull, and F. R. Merritt, "Spin-3/2 iron ferromagnet: Its Mössbauer and magnetic properties," *Phys. Rev.*, vol. 155, no. 2, pp. 563–566, 1967, doi: 10.1103/PhysRev.155.563.

[4] J. S. Miller *et al.*, "Ferromagnetic Behavior of [Fe(C5Me5)2]+[TCNE]- Structural and Magnetic Characterization of Decamethylferrocenium Tetracyanoethenide, and Decamethylferrocenium Pentacyanopropenide," *J. Am. Chem. Soc.*, vol. 109, no. 8, pp. 769–781, 1987.

[5] J. M. Manriquez, G. T. Yee, R. S. Mclean, A. J. Epstein, and J. S. Millert, "A Room-Temperature Molecular / Organic-Based Magnet," vol. 2, no. 22, pp. 22–24, 1988.

[6] M. N. Leuenberger and D. Loss, "Quantum computing in molecular magnets," *Nature*, vol. 410, no. 6830, pp. 789–793, 2001, doi: 10.1038/35071024.

[7] M. A. Novak, R. Sessoli, A. Caneschi, and D. Gatteschi, "Magnetic properties of a Mn cluster organic compound," *J. Magn. Magn. Mater.*, vol. 146, no. 1–2, pp. 211–213, 1995, doi: 10.1016/0304-8853(94)00860-4.

[8] J. R. Friedman, M. P. Sarachik, J. Tejada, and R. Ziolo, "Macroscopic measurement of resonant magnetization tunneling in high-spin molecules," *Phys. Rev. Lett.*, vol. 76, no. 20, pp. 3830–3833, 1996, doi: 10.1103/PhysRevLett.76.3830.

[9] L. Thomas, F. Lionti, R. Ballou, D. Gatteschi, R. Sessoli, and B. Barbara, "Macroscopic quantum tunnelling of magnetization in a single crystal of nanomagnets," *Nature*, vol. 383, no. 6596. pp. 145–147, 1996, doi: 10.1038/383145a0.

[10] G. Tosi *et al.*, "Silicon quantum processor with robust long-distance qubit couplings," *Nat. Commun.*, vol. 8, no. 1, pp. 1–11, 2017, doi: 10.1038/s41467-017-00378-x.

[11] P. I. Chemistry, *S. F. A. Kettle (auth.) Physical Inorganic Chemistry_ A Coordination Chemistry Approach 1996*. 2013.

[12] H. Gregson, A. K. Gregson, D. M. Doddrell, and P. C. Healylb, "Low-Temperature Magnetic Properties of Three Vanadium(III) and Manganese(III) ß-Diketonate Complexes," 1978. Accessed: Jul. 29, 2020. [Online]. Available: https://pubs.acs.org/sharingguidelines.

[13] Y. Yu, "ABSTRACT CALCULATION OF EXCHANGE AND ANISOTROPY ENERGIES IN SINGLE MOLECULE MAGNETS."

[14] J. Sun, J. W. Furness, and Y. Zhang, "Density functional theory," in *Mathematical Physics in Theoretical Chemistry*, Elsevier, 2019, pp. 119–159.

[15] A. D. Becke, "Hartree–Fock exchange energy of an inhomogeneous electron gas," *Int. J. Quantum Chem.*, vol. 23, no. 6, pp. 1915–1922, Jun. 1983, doi: 10.1002/qua.560230605.

[16] A. D. Becke, "A new inhomogeneity parameter in density-functional theory," *J. Chem. Phys.*, vol. 109, no. 6, pp. 2092–2098, Aug. 1998, doi: 10.1063/1.476722.

[17] M. R. Pederson and S. N. Khanna, "Magnetic anisotropy barrier for spin tunneling in Mn12O12molecules," *Phys. Rev. B - Condens. Matter Mater. Phys.*, vol. 60, no. 13, pp. 9566–9572, Oct. 1999, doi: 10.1103/PhysRevB.60.9566.

[18] M. R. Pederson, D. V. Porezag, J. Kortus, and D. C. Patton, "Strategies for Massively Parallel Local-Orbital-Based Electronic Structure Methods," in *Computer Simulation of Materials at Atomic Level*, Wiley-VCH Verlag GmbH & Co. KGaA, 2005, pp. 197–218.

[19] T. Baruah and M. R. Pederson, "Density functional study of the conformers of Co4-based single-molecule magnet," *Int. J. Quantum Chem.*, vol. 93, no. 5, pp. 324–331, Jun. 2003, doi: 10.1002/qua.10491.

[20] J. Kortus, M. R. Pederson, T. Baruah, N. Bernstein, and C. S. Hellberg, "Density functional studies of single molecule magnets," *Polyhedron*, vol. 22, no. 14–17, pp. 1871–1876, 2003, doi: 10.1016/S0277-5387(03)00160-8.

[21] "Phys. Rev. B 41, 7453 (1990) - Variational mesh for quantum-mechanical simulations."

https://journals.aps.org/prb/abstract/10.1103/PhysRevB.41.7453 (accessed Jul. 29, 2020).

[22] D. Porezag and M. R. Pederson, “Optimization of Gaussian basis sets for density-functional calculations,” *Phys. Rev. A - At. Mol. Opt. Phys.*, vol. 60, no. 4, pp. 2840–2847, Oct. 1999, doi: 10.1103/PhysRevA.60.2840.

[23] R. P. Feynman, “Forces in molecules,” *Phys. Rev.*, vol. 56, no. 4, pp. 340–343, Aug. 1939, doi: 10.1103/PhysRev.56.340.

[24] P. Pulay, “Ab initio calculation of force constants and equilibrium geometries in polyatomic molecules,” *Mol. Phys.*, vol. 17, no. 2, pp. 197–204, 1969, doi: 10.1080/00268976900100941.

[25] W. Kohn and L. J. Sham, “PHYSICAL REVIEW Self-Consistent Equations Including Exchange and Correlation Effects*.”

[26] Y. Yamamoto, A. Salcedo, C. M. Diaz, M. S. Alam, T. Baruah, and R. Zope, “Assessing the effect of regularization on the molecular properties predicted by SCAN and self-interaction corrected SCAN meta-GGA,” *Phys. Chem. Chem. Phys.*, 2020, doi: 10.1039/D0CP02717K.

[27] X. N. Yao *et al.*, “Two-coordinate Co(II) imido complexes as outstanding single-molecule magnets,” *J. Am. Chem. Soc.*, vol. 139, no. 1, pp. 373–380, Jan. 2017, doi: 10.1021/jacs.6b11043.

[28] A. Escuer, M. Font-Bardia, S. B. Kumar, X. Solans, and R. Vicente, “Two new nickel (II) cubane compounds derived from pyridine-2-methoxide (Pym).,” *Polyhedron*, vol. 18, pp. 909–914, 1999.

[29] E. C. Yang *et al.*, “Fast magnetization tunneling in tetranickel(II) single-molecule magnets,” *Inorg. Chem.*, vol. 45, no. 2, pp. 529–546, 2006, doi: 10.1021/ic050093r.

[30] C. Cao, S. Hill, and H. P. Cheng, “Strongly correlated electrons in the [Ni(hmp)(ROH)X]4 single molecule magnet: A DFT+U study,” *Phys. Rev. Lett.*, vol. 100, no. 16, p. 167206, Apr. 2008, doi: 10.1103/PhysRevLett.100.167206.

[31] K. Park, E. C. Yang, and D. N. Hendrickson, “Electronic structure and magnetic

anisotropy for nickel-based molecular magnets," *J. Appl. Phys.*, vol. 97, no. 10, pp. 2003–2006, 2005, doi: 10.1063/1.1859972.

[32] G. Kresse and J. Furthmüller, "Efficiency of ab-initio total energy calculations for metals and semiconductors using a plane-wave basis set," *Comput. Mater. Sci.*, vol. 6, no. 1, pp. 15–50, Jul. 1996, doi: 10.1016/0927-0256(96)00008-0.

[33] P. E. Blöchl, "Projector augmented-wave method," *Phys. Rev. B*, vol. 50, no. 24, pp. 17953–17979, Dec. 1994, doi: 10.1103/PhysRevB.50.17953.

[34] J. P. Perdew and K. Burke, "Generalized gradient approximation for the exchange-correlation hole of a many-electron system," *Phys. Rev. B - Condens. Matter Mater. Phys.*, vol. 54, no. 23, pp. 16533–16539, Dec. 1996, doi: 10.1103/PhysRevB.54.16533.

[35] J. Klime, D. R. Bowler, and A. Michaelides, "Van der Waals density functionals applied to solids," *Phys. Rev. B - Condens. Matter Mater. Phys.*, vol. 83, no. 19, p. 195131, May 2011, doi: 10.1103/PhysRevB.83.195131.

[36] H. J. Monkhorst and J. D. Pack, "Special points for Brillouin-zone integrations," *Phys. Rev. B*, vol. 13, no. 12, pp. 5188–5192, Jun. 1976, doi: 10.1103/PhysRevB.13.5188.

[37] "PSTRESS - Vaspwiki." https://www.vasp.at/wiki/index.php/PSTRESS (accessed Jul. 29, 2020).

[38] "First-principles calculations of the electronic structure and spectra of strongly correlated systems: the LDA+ U method - IOPscience." https://iopscience.iop.org/article/10.1088/0953-8984/9/4/002 (accessed Jul. 29, 2020).

[39] B. Morosin and A. Narath, "X-ray diffraction and nuclear quadrupole resonance studies of chromium trichloride," *J. Chem. Phys.*, vol. 40, no. 7, pp. 1958–1967, Apr. 1964, doi: 10.1063/1.1725428.

[40] L. L. Handy and N. W. Gregory, "Structural Properties of Chromium(III) Iodide and Some Chromium(III) Mixed Halides," *J. Am. Chem. Soc.*, vol. 74, no. 4, pp. 891–893, Feb. 1952, doi: 10.1021/ja01124a009.

[41] W. B. Zhang, Q. Qu, P. Zhu, and C. H. Lam, "Robust intrinsic ferromagnetism and half

semiconductivity in stable two-dimensional single-layer chromium trihalides," *J. Mater. Chem. C*, vol. 3, no. 48, pp. 12457–12468, Dec. 2015, doi: 10.1039/c5tc02840j.

[42] H. Takahashi *et al.*, "Pressure-induced superconductivity in the iron-based ladder material BaFe 2 S 3," *Nat. Mater.*, vol. 14, no. 10, pp. 1008–1012, Oct. 2015, doi: 10.1038/nmat4351.

[43] A. O. Fumega, S. Blanco-Canosa, H. Babu-Vasili, J.-S. Zhou, F. Rivadulla, and V. Pardo, "Electronic structure and magnetic exchange interactions of Cr-based van der Waals ferromagnets. A comparative study between CrBr3 and Cr2Ge2Te6," pp. 1–8, 2020, [Online]. Available: http://arxiv.org/abs/2004.11789.

[44] T. Kanomata, T. Tsuda, H. Yasui, and T. Kaneko, "Effect of pressure on the Curie temperature of CoCr2O4," *Phys. Lett. A*, vol. 134, no. 3, pp. 196–198, Dec. 1988, doi: 10.1016/0375-9601(88)90820-1.

[45] H. Yoshida, J. Chiba, T. Kaneko, Y. Fujimori, and S. Abe, "Pressure effect on the Curie temperature of CrBr3," *Phys. B Condens. Matter*, vol. 237–238, pp. 525–526, 1997, doi: 10.1016/S0921-4526(97)00207-X.

[46] W. Geertsma and D. Khomskii, "Influence of side groups on 90° superexchange: A modification of the Goodenough-Kanamori-Anderson rules," *Phys. Rev. B - Condens. Matter Mater. Phys.*, vol. 54, no. 5, pp. 3011–3014, Aug. 1996, doi: 10.1103/PhysRevB.54.3011.

[47] A. O. Fumega *et al.*, "Electronic structure and magnetic exchange interactions of Cr-based van der Waals ferromagnets. A comparative study between $CrBr_3$ and $Cr_2Ge_2Te_6$," *J. Mater. Chem. C*, 2020, doi: 10.1039/D0TC02003F.

[48] R. Albaridy, A. Manchon, and U. Schwingenschlögl, "Tunable magnetic anisotropy in Cr–trihalide Janus monolayers," *J. Phys. Condens. Matter*, vol. 32, no. 35, p. 355702, 2020, doi: 10.1088/1361-648x/ab8986.

[49] S. Mondal *et al.*, "Effect of hydrostatic pressure on ferromagnetism in two-dimensional CrI3," *Phys. Rev. B*, vol. 99, no. 18, p. 180407, 2019, doi: 10.1103/PhysRevB.99.180407.

Vita

Md Shamsul Alam was born in Dhaka, Bangladesh. He completed his Bachelor of Science and Masters of Science in Physics from University of Dhaka which is the top ranked university in Bangladesh. He joined at the University of Texas at El Paso in January 2018 as a graduate student. He got the opportunity to work as a Teaching Assistant and Research Assistant in the Computational Science Department at the University of Texas at El Paso.